



HAL
open science

Numerical homogenization of fiber reinforced layer in large elastic deformation using a decoupled iterative method

Sarra Karoui, Khalil Mansouri, Yves Renard, Makrem Arfaoui, Thomas Homolle, Philippe Bussetta

► To cite this version:

Sarra Karoui, Khalil Mansouri, Yves Renard, Makrem Arfaoui, Thomas Homolle, et al.. Numerical homogenization of fiber reinforced layer in large elastic deformation using a decoupled iterative method. 2023. hal-04134644

HAL Id: hal-04134644

<https://hal.science/hal-04134644>

Preprint submitted on 20 Jun 2023

HAL is a multi-disciplinary open access archive for the deposit and dissemination of scientific research documents, whether they are published or not. The documents may come from teaching and research institutions in France or abroad, or from public or private research centers.

L'archive ouverte pluridisciplinaire **HAL**, est destinée au dépôt et à la diffusion de documents scientifiques de niveau recherche, publiés ou non, émanant des établissements d'enseignement et de recherche français ou étrangers, des laboratoires publics ou privés.

Numerical homogenization of fiber reinforced layer in large elastic deformation using a decoupled iterative method

Karoui S. ^{*} Mansouri K. [†] Renard Y. [‡] Arfaoui M. [§] Homolle T. [¶] Bussetta P. ^{||}

June 20, 2023

Abstract

We propose a procedure to approximate the large elastic deformations of a fiber reinforced layer by a two-scale decoupled homogenization numerical procedure. The nonlinear micro and macroscopic scales are strongly coupled in most homogenization methods which is very costly. Our method consists in decoupling the micro and macro scales by considering separate boundary value problems and an intermediate anisotropic constitutive law optimised over a training set. We propose an iterative procedure based on this method which allows to improve the quality of the approximation to get closer to the coupled homogenization and keeping a reasonable computational cost. We perform representative numerical studies for a layer with heterogeneous hyperelastic material in order to demonstrate the capability and reliability of the proposed method and test several intermediate constitutive laws.

Keywords: hyperelasticity, decoupled homogenization method, composite layer, large deformation.

1 Introduction

The existence of fiber-reinforced rubber-like composites in natural and artificial materials and structures has long been known and has been the subject of study in many fields including manufacturing, plants, geomechanics, and biomechanics. At a macroscale, some fiber reinforced rubber-like composites, such as soft tissues [27], appear homogeneous, yet at a specific microscale, they exhibit fibrous microstructure behaviour. At a macroscopic observation scale, several other reinforced rubber-like composites, such as the fiber-reinforced layers in the tyres that serve as the subject of this study (see also [53]), appear heterogeneous. These materials and structures are classified as fiber-embedded composites and can be physically represented as a pliable matrix material with aligned cylindrical stiffer fiber inclusions. Two methodologies can be used to model the mechanical behaviour of these materials: micro-mechanical [64] and macro-mechanical phenomenology [116]. The micro-macro or homogenization technique is useful for comprehending and

^{*}Univ Lyon, INSA Lyon, CNRS UMR 5259, LaMCoS, F-69621, France, email: sarra.karoui@insa-lyon.fr

[†]Université de Tunis El Manar, École Nationale d'Ingénieurs de Tunis, LR-11-ES19, Laboratoire de Mécanique Appliquée et Ingénierie, Tunis 1002, Tunisie, email: khalil.mansouri@enit.utm.tn

[‡]Univ Lyon, INSA Lyon, CNRS UMR 5259, LaMCoS, F-69621, France, email: yves.renard@insa-lyon.fr

[§]Université de Tunis El Manar, École Nationale d'Ingénieurs de Tunis, LR-11-ES19, Laboratoire de Mécanique Appliquée et Ingénierie, Tunis 1002, Tunisie, email: makrem.arfaoui@enit.utm.tn

[¶]Michelin, Technology centre, Ladoux, France, email: thomas.homolle@michelin.com

^{||}Michelin, Technology centre, Ladoux, France, email: philippe.bussetta@michelin.com

designing the physical behaviour of materials. However, this method is expensive for commercial use, particularly for nonlinear material behaviour [28]. The macro-mechanical phenomenological continuum technique, where the model's parameters are calibrated using data from macroscopic experiments, is an effective and straightforward way to construct constitutive equations [116]. Despite having these desirable characteristics, these phenomenological models are hampered by a lack of actual knowledge about the microstructure of fiber-reinforced rubber-like composites.

Thus, the scientific objective of this paper is the development of a mechanical and numerical methodology linking the micromechanical and the macromechanical phenomenological approaches while keeping their advantages and reducing their inconveniences. This is the decoupled homogenization method. To do this, the fiber and the matrix will be considered as hyperelastic materials. This is a first approximation which can be enriched in other works.

Classical homogenization theory [18, 19, 33, 92, 93, 5] has long been an essential tool to characterize the behaviour of composite materials with periodic or quasi-periodic microstructures and to derive numerical approximations at reasonable costs, especially in the context of linear materials where homogenized constitutive laws can often be identified with a limited number of parameters to be determined. Homogenization methods, one of the first multiscale approaches in mechanics, can be classified based on problem formulation. These classifications include concurrent methods, where both scales are simultaneously addressed within the problem formulation, allowing for the utilization of different length and time scales in a single domain [24]. Hierarchical methods establish a hierarchical connection between scales, coupling distinct scales within the same domain region [112]. Hybrid methods combine elements from different methods, leveraging their respective strengths. Examples of hybrid methods include multigrid methods, the generalized finite element method, wavelet-based methods, and quasi-continuum methods [107], [59] and [80]. In recent years, there has been a significant increase in contributions that have further developed computational homogenization (CH) methods or utilized them for multiscale analysis in materials. These advancements have led to numerous applications in various areas, including porous media [106];[127];[122], cellular materials [67];[47], polycrystalline metals [100], technical textiles [23], granular materials [52], trabecular bone [121], composite plates [36], and Li-ion battery cells [91]. These examples highlight the diverse range of materials and systems where CH methods have been successfully applied for multiscale analysis, driving advancements in the field of material science and engineering.

In the context of the homogenization of hyperelastic composites [39, 40, 72] apart from very specific situations in terms of constitutive laws used at the microscopic scale and even in terms of loading (see [9, 11, 34, 35, 12, 54]), it is not possible to identify the homogenized law in the nonlinear case which makes the decoupling between the micro and macroscopic scales impossible to reach. This has given rise to the development of the so-called computational homogenization, which has motivated a very large number of studies [14, 66, 60]. We refer for instance to the monograph [123] and the references therein for an overview of computational homogenization techniques. A classical numerical strategy to keep the micro-macro coupling is the use of the so called FE² approximation [83, 104, 21, 22, 113]. This type of strategy (also called multilevel finite element method) consists in solving a finite element approximation on the RVE (representative volume element of the microstructure) at each integration point of a finite element method for the macroscopic problem. It gives very good results, but is extremely expensive in terms of computational resources, even when model reduction strategies are applied (as proposed for instance in [125, 61, 38, 16]). A discussion of the extension to second order homogenization for an enhanced accuracy can be found for instance in [77] and the references therein, however, this kind of strategy is even more computationally expensive which can represent a serious obstacle to its use.

Within this frame of reference, the decoupled numerical method introduced by Terada et al.

[111] allows to recover computational cost comparable to a classical structural mechanics calculation with a homogeneous material (see also [81, 90] for further developments). This is at the cost of an additional approximation on the homogenized law whose shape is preselected with a more or less important number of parameters. This law aims at characterizing the global response of the micro-structure at the RVE level, at least in the solicitation range of interest for the macroscopic level. The method can be used either with simple homogenized laws, in the case such a specific simple law can be expected, or either with more complex or even fully parametric laws. A possibility in order to identify a fully parametric law is to take advantage of the approximation property of artificial neural network (see [50, 48]). An optimization of the homogenized law parameters is performed off-line on a training set composed of numerical experiments coming from a finite element approximation of the boundary value problem (BVP) defined at the micro-scale on the RVE. The shape of the chosen homogenized law is obviously crucial for the proper functioning and efficiency of the method. Once parameters of the homogenized law have been identified, it can be used to represent the micro-scale response and then to evaluate the macro-scale response. In the context of modern continuum mechanics [116], Rivlin developed in a series of papers [85, 87, 88, 89, 86] a formalism for the modelling of large elastic deformations of isotropic materials. The main idea of this theory is based on Georges Green’s method established in 1840 [115] by modelling the elastic behaviour with a strain energy function: the elastic material is named hyperelastic material. The effect of fiber reinforced material was first analyzed by resolving some boundary value problems of an isotropic hyperelastic matrix reinforced with inextensible cords [1]. This exact analytical approach uses the semi-inverse method [115]. Another way to model the effect of fiber reinforced material was initiated by [17]. The strain energy is assumed to be a function of some strain invariants that are used to model the fibres directions effect with some structural tensors [57, 6]. This phenomenological approach was used to develop some popular hyperelastic anisotropic models [120, 7, 49, 42, 43, 44]. The analysis of the ellipticity, convexity, polyconvexity or other inequality [56] of constitutive law was extended to anisotropy in [96, 2] among others.

Note that the decoupled homogenization numerical method discussed in reference [111] does not address the interface problem. Recent studies such as [102], [46], [101], and [31] have employed innovative multiscale approaches to address the complexities associated with interface and crack behaviour.

The main objective of this study is to propose a computational homogenization strategy for a fiber reinforced layer in large elastic deformation having the best possible compromise in term of computational cost and reliability. For this purpose, based on the decoupled method of Terada et al. [111], we perform a comparison of two different homogenized transversely isotropic hyperelastic potentials with moderate number of parameters. Moreover, we introduce an iteration method to improve the approximation error of the decoupled homogenization strategy. This method, by taking into account the deformation state of the structure at the macroscopic scale, allows to better approach the coupled FE^2 method while keeping a much lower numerical cost.

The paper is organized as follows. Section 2 introduces the homogenization in large deformations. Section 3 describes the decoupled computational homogenization and a comparison of some different homogenized potentials in term of a local error. In section 4, the tests are on the macro scale on a fiber reinforced layer. A comparison is done both in term of local error and global error with a fully discretized heterogeneous layer. We introduce in section 5 our iterative method and test its effectiveness in term of local and global error. Finally, a conclusion is drawn in section 6.

2 Two-scale boundary-value problem homogenization

In order to introduce the two-scale homogenization for the large deformation of a micro-structured composite material, we describe first the macro-scale description, then the micro-scale one and finally the coupling between the two scales.

2.1 Macro-scale description

Consider a continuum body that occupies the reference configuration $\tilde{\mathcal{B}}_0$ with the boundary $\partial\tilde{\mathcal{B}}_0$ and the outward unit normal vector $\tilde{\mathbf{N}}$ where each point is labeled by the macro-scale reference position vector $\mathbf{X} \in \tilde{\mathcal{B}}_0$. It is mapped to the spatial current configuration $\tilde{\mathcal{B}}_t$ with the boundary $\partial\tilde{\mathcal{B}}_t$ and the surface normal unit vector $\tilde{\mathbf{n}}$, labeled by its current position \mathbf{x} via the nonlinear deformation function $\tilde{\varphi}(\mathbf{X}) = \tilde{\mathbf{u}}(\mathbf{X}) + \mathbf{X}$, where $\tilde{\mathbf{u}}$ being the macro-scale displacement field, written as $\mathbf{x} = \tilde{\varphi}(\mathbf{X}) \in \tilde{\mathcal{B}}_t$ (see fig. 1). The macro-scale deformation gradient $\tilde{\mathbf{F}} = \mathbf{Grad}_{\mathbf{X}}(\tilde{\varphi}(\mathbf{X}))$ linearly relates a reference line element $d\mathbf{X} \in \tilde{\mathcal{B}}_0$ to a spatial current line element $d\mathbf{x} \in \tilde{\mathcal{B}}_t$, by

$$d\mathbf{x} = \tilde{\mathbf{F}} \cdot d\mathbf{X}. \quad (1)$$

For a macroscopic heterogeneous body, subjected to loading and constraints and in the absence of inertia effects, the macro-scale equilibrium equation is expressed as

$$\nabla_{\mathbf{X}} \cdot \tilde{\mathbf{P}} + \tilde{\mathbf{b}} = \mathbf{0} \text{ in } \tilde{\mathcal{B}}_0, \quad (2)$$

where $\tilde{\mathbf{P}}$ is the macro-scale first Piola–Kirchhoff stress tensor and $\tilde{\mathbf{b}}$ is the body forces on the reference configuration $\tilde{\mathcal{B}}_0$. Here, $\nabla_{\mathbf{X}}$ denotes the divergence operator with respect to material macro-scale coordinates. The body is subjected to Neumann and Dirichlet boundary conditions

$$\begin{aligned} \tilde{\mathbf{P}} \cdot \tilde{\mathbf{N}} &= \tilde{\mathbf{T}}_0 \text{ on } \partial\tilde{\mathcal{B}}_0^N, \\ \tilde{\mathbf{u}} &= \tilde{\mathbf{u}}_0 \text{ on } \partial\tilde{\mathcal{B}}_0^D, \end{aligned} \quad (3)$$

where $\tilde{\mathbf{T}}_0$ is the given applied density on the reference configuration, $\tilde{\mathbf{u}}_0$ the prescribed displacement on $\partial\tilde{\mathcal{B}}_0^D$ and $\{\partial\tilde{\mathcal{B}}_0^N, \partial\tilde{\mathcal{B}}_0^D\}$ are partitions of $\partial\tilde{\mathcal{B}}_0$.

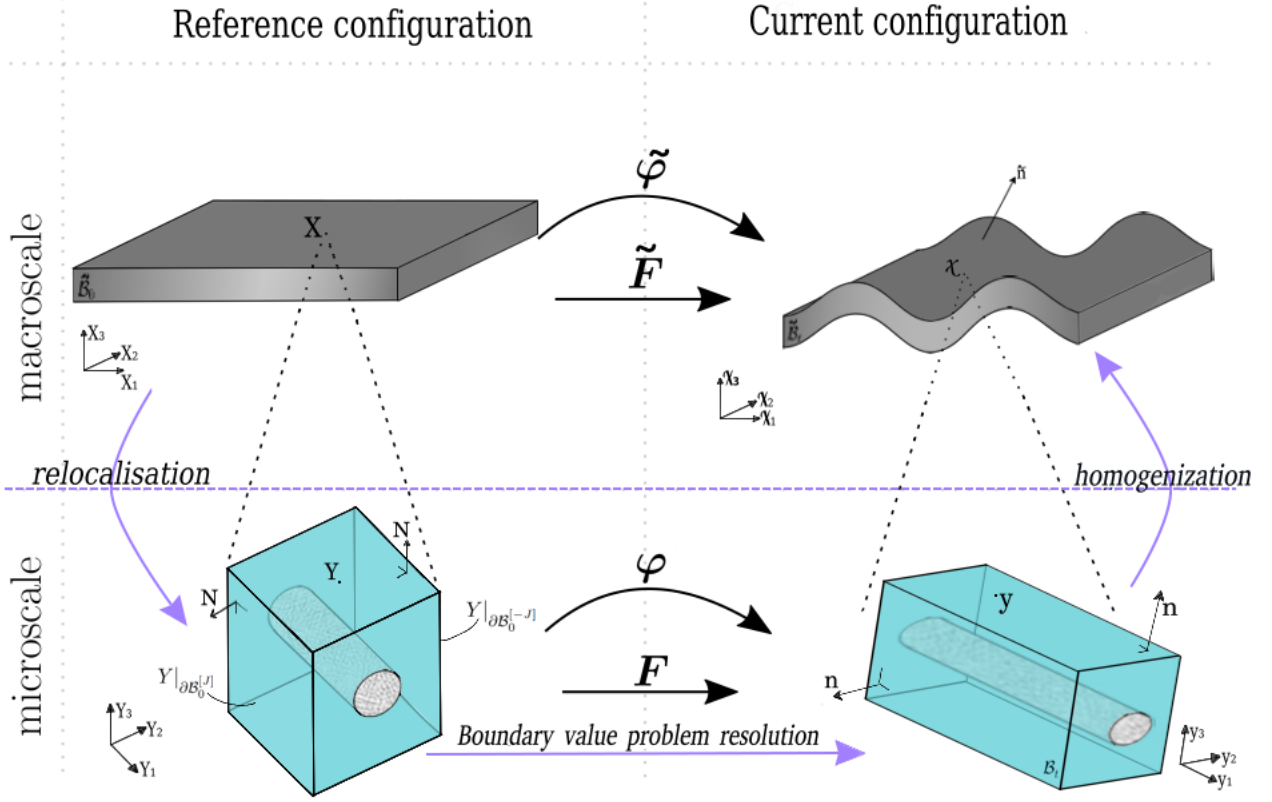


Figure 1: Two-scale coupled homogenization

2.2 Micro-scale description

The mechanical behaviour of the material micro-structure is identified through a representative volume element (RVE). Ideally this RVE should include a sampling of all micro-structural heterogeneities that occur in the composite at a length scale that should be smaller than the characteristic length of the relevant macroscopic field variation, but sufficiently larger than the micro-scale physics and micro-fluctuations. In particular, it is very important in the homogenization of a fibrous material that the fiber/matrix ratio is maintained on both scales, see classical textbooks on homogenization theory [65, 25].

In this work the representative volume element (RVE) is usually taken to be a unit cell, due to the scale independence of the equation and boundary conditions and by neglecting the effects due to the onset of instability phenomena [58], [30], [32]. The spatial position, denoted \mathbf{Y} , in the micro-scale reference configuration \mathcal{B}_0 of the unit cell domain, and the spatial position \mathbf{y} in the micro-scale current configuration \mathcal{B}_t , are introduced. These two positions are related by the micro-scale deformation as follows:

$$\mathbf{y} = \varphi(\mathbf{X}; \mathbf{Y}) = \mathbf{Y} + \mathbf{w}(\mathbf{X}; \mathbf{Y}), \quad (4)$$

where

$$\mathbf{w}(\mathbf{X}; \mathbf{Y}) = \tilde{\mathbf{H}}(\mathbf{X}) \cdot \mathbf{Y} + \mathbf{u}^*(\mathbf{X}; \mathbf{Y}) + \mathbf{c}(\mathbf{X}), \quad (5)$$

is the micro-scale displacement of the unit cell, $\tilde{\mathbf{H}}$ is the macro-scale displacement gradient defined as $\tilde{\mathbf{H}}(\mathbf{X}) = \nabla_{\mathbf{X}} \tilde{\mathbf{u}}(\mathbf{X})$, \mathbf{u}^* is the fluctuation displacement, in our case assumed to be exposed to

the periodic boundary condition on the RVE external boundary $\partial\mathcal{B}_0$ and \mathbf{c} is a constant vector independent of \mathbf{Y} , derived from the integration of the micro-scale deformation gradient defined as

$$\mathbf{F}(\mathbf{X}; \mathbf{Y}) = \nabla_{\mathbf{Y}}\varphi(\mathbf{X}; \mathbf{Y}) = \nabla_{\mathbf{Y}}\mathbf{w}(\mathbf{X}; \mathbf{Y}) + \mathbb{1} = \mathbf{H}(\mathbf{X}; \mathbf{Y}) + \mathbb{1}, \quad (6)$$

where $\mathbb{1}$ is the metric tensor (whose components form the identity matrix in a orthonormal reference frame) and H is the micro-scale displacement gradient given by

$$\mathbf{H}(\mathbf{X}; \mathbf{Y}) = \nabla_{\mathbf{Y}}\mathbf{w}(\mathbf{X}; \mathbf{Y}) = \tilde{\mathbf{H}}(\mathbf{X}) + \nabla_{\mathbf{Y}}\mathbf{u}^*(\mathbf{X}; \mathbf{Y}), \quad (7)$$

where $\tilde{\mathbf{H}} = \frac{1}{|\mathcal{B}_0|} \int_{\mathcal{B}_0} \mathbf{H} d\mathbf{V}$ and $|\mathcal{B}_0|$ is the reference volume of the RVE (in our case, $|\mathcal{B}_0| = 1$).

The macro-homogeneous deformation tensor $\tilde{\mathbf{F}}$ is related to the micro-scale deformation gradient tensor for every point at the micro-scale by

$$\mathbf{F}(\mathbf{X}; \mathbf{Y}) = \tilde{\mathbf{F}}(\mathbf{X}) + \nabla_{\mathbf{Y}}\mathbf{u}^*(\mathbf{X}; \mathbf{Y}). \quad (8)$$

In the absence of body forces, the micro-scale self-equilibrium equation for the unit cell RVE in terms of the micro-scale first Piola–Kirchhoff stress tensor \mathbf{P} and its response function $\mathcal{F}(\mathbf{F})$ is given by

$$\begin{cases} \nabla_{\mathbf{Y}} \cdot \mathbf{P} = 0 & \text{in } \mathcal{B}_0 \\ \mathbf{P} = \mathcal{F}(\mathbf{F}) & \text{in } \mathcal{B}_0 \end{cases} \quad (9)$$

subjected to periodic boundary conditions

$$\mathbf{w}|_{\partial\mathcal{B}_0^{[J]} - \mathbf{w}|_{\partial\mathcal{B}_0^{[-J]}} = \mathbf{w}^{[J]} - \mathbf{w}^{[-J]} = \tilde{\mathbf{H}} \cdot \mathbf{L}^{[J]} \quad \text{on } \partial\mathcal{B}_0^{[J]} \quad (J = 1, 2, 3), \quad (10)$$

where $\partial\mathcal{B}_0^{[J]}$ and $\partial\mathcal{B}_0^{[-J]}$ indicate a pair of opposite external faces of the RVE (see fig. 1) and \mathbf{L} is called the side vector connecting the material points on opposite external forces of the RVE, and the periodic boundary condition are defined as

$$\mathbf{L}^{[J]} := \mathbf{Y}|_{\partial\mathcal{B}_0^{[J]}} - \mathbf{Y}|_{\partial\mathcal{B}_0^{[-J]}} \quad (J = 1, 2, 3). \quad (11)$$

Here, $\nabla_{\mathbf{Y}}$ denotes the divergence operator with respect to material micro-scale coordinates and \mathcal{F} is a functional defining the constitutive law.

2.3 Micro-macro coupling

The first order coupling homogenization is based on the idea of computing the overall response of the micro-scale problem, in particular the macro-scale first Piola–Kirchhoff stress tensor $\tilde{\mathbf{P}}$, by prescribing the macroscopic deformation gradient $\tilde{\mathbf{F}}$ onto the micro-problem. Microscopic quantities are related to their macroscopic counterparts through volume averaging over the RVE [40, 72, 55].

The macro-scale deformation gradient can be written as the volume average of the corresponding micro-scale deformation gradient over the RVE derived from (6)

$$\tilde{\mathbf{F}} = \frac{1}{|\mathcal{B}_0|} \int_{\mathcal{B}_0} \mathbf{F} d\mathbf{V} = \tilde{\mathbf{H}} + \mathbb{1}. \quad (12)$$

The insertion of the micro-scale deformation gradient tensor (8) into (12) leads to

$$\frac{1}{|\mathcal{B}_0|} \int_{\mathcal{B}_0} \mathbf{F} d\mathbf{V} = \tilde{\mathbf{F}} + \frac{1}{|\mathcal{B}_0|} \int_{\mathcal{B}_0} \nabla_{\mathbf{Y}}\mathbf{u}^*(\mathbf{X}; \mathbf{Y}) d\mathbf{V} = \tilde{\mathbf{F}} + \frac{1}{|\mathcal{B}_0|} \int_{\partial\mathcal{B}_0} \mathbf{u}^*(\mathbf{X}; \mathbf{Y}) \otimes \mathbf{N} d\mathbf{A}, \quad (13)$$

where we use the divergence theorem to transform the volume integral to surface integral over the undeformed boundary $\partial\mathcal{B}_0$ of the RVE with outward normal vector \mathbf{N} .

It is clear that in order to satisfy the relation between the micro-scale deformation gradient tensor and the macro-scale one (10), the contribution of the micro-fluctuation field $\mathbf{u}^*(X; Y)$ must vanish at the macro level, which means to prescribe the following adequate boundary conditions

$$\mathbf{u}^*|_{\partial\mathcal{B}_0^{[J]}} = \mathbf{u}^*|_{\partial\mathcal{B}_0^{[-J]}} \quad (J = 1, 2, 3). \quad (14)$$

The macro-scale first Piola–Kirchhoff stress tensor \tilde{P} can be defined as the volume average of the corresponding micro-scale stress P over the unit cell RVE as

$$\tilde{\mathbf{P}} = \frac{1}{|\mathcal{B}_0|} \int_{\mathcal{B}_0} \mathbf{P} d\mathbf{V}. \quad (15)$$

Considering the periodicity condition, the micro Piola traction vector \mathbf{T} satisfies an anti-periodicity conditions on the unit cell boundary $\partial\mathcal{B}_0$ with \mathbf{N} being the outward unit normal vector on the corresponding surface in the reference configuration

$$\mathbf{T}^{[J]} + \mathbf{T}^{[-J]} = 0 \quad \text{where } \mathbf{T}^{[J]} = \mathbf{P} \cdot \mathbf{N}^{[J]}, \quad (16)$$

from which the average Piola traction vector can be derived

$$\tilde{\mathbf{T}}_i^{[J]} = \tilde{\mathbf{P}}_{iJ} = \mathbf{N}^{[i]} \cdot \tilde{\mathbf{T}}^{[J]} = \mathbf{N}^{[i]} \cdot (\tilde{\mathbf{P}} \cdot \mathbf{N}^{[J]}) = \mathbf{N}^{[i]} \cdot \left(\frac{1}{|\partial\mathcal{B}_0|} \int_{\partial\mathcal{B}_0} \mathbf{P} \cdot \mathbf{N}^{[J]} d\mathbf{A} \right) = \frac{1}{|\partial\mathcal{B}_0^{[J]}|} \int_{\partial\mathcal{B}_0^{[J]}} \mathbf{T}_i^{[J]} d\mathbf{s}, \quad (17)$$

where $|\partial\mathcal{B}_0^{[J]}|$ is the area of the RVE boundary $\partial\mathcal{B}_0^{[J]}$ and $\tilde{\mathbf{P}}_{iJ}$ is the iJ component of the macro-scale first Piola–Kirchhoff stress tensor, the area average of the corresponding micro-scale Piola traction vector $\mathbf{T}_i^{[J]}$ at the unit cell boundary $\partial\mathcal{B}_0^{[J]}$. This relation is of great interest for the numerical computation of $\tilde{\mathbf{P}}$.

A standard requirement is the satisfaction of the Hill–Mandel condition [40, 55] that requires the volume average of the variation of work performed on the RVE to be equal to the increment of local work on the macro-scale, formulated as

$$\frac{1}{|\mathcal{B}_0|} \int_{\mathcal{B}_0} \mathbf{P} : \delta\mathbf{F}^T d\mathbf{V} = \tilde{\mathbf{P}} : \delta\tilde{\mathbf{F}}^T. \quad (18)$$

The boundary conditions of the RVE that satisfy the Hill–Mandel condition must be determined in order to solve the micro-problem. These are determined using Hill’s lemma

$$\frac{1}{|\mathcal{B}_0|} \int_{\mathcal{B}_0} \mathbf{P} : \delta\mathbf{F}^T d\mathbf{V} - \tilde{\mathbf{P}} : \delta\tilde{\mathbf{F}}^T = \int_{\partial\mathcal{B}_0} [\delta\varphi - \delta\tilde{\mathbf{F}} \cdot \mathbf{Y}] \cdot [\mathbf{P} \cdot \mathbf{N} - \tilde{\mathbf{P}} \cdot \mathbf{N}] d\mathbf{A}. \quad (19)$$

In our case, the periodic displacement, anti-periodic traction boundary conditions and (15) are sufficient to satisfy the Hill–Mandel condition.

The coupled micro-macro homogenized problem can be summarized as follows; the micro-scale BVP is to be solved for each $\mathbf{X} \in \tilde{\mathcal{B}}_0$ for the set of solutions \mathbf{w} from (5), \mathbf{F} from (6), H from (7) that satisfies the micro-scale equilibrium equation (9) along with the periodic condition (10), while the macro-scale BVP is for $\tilde{\mathbf{F}}$ (12), $\tilde{\mathbf{P}}$ (15) that satisfies (12), (15) and (2). It is noted that the micro-scale BVP can be solved only if the macro-scale solution is given and vice versa.

This coupled homogenization method allows to define analytical effective behaviour of heterogeneous materials for simple and special classes of uniform boundary conditions and materials constituents models behaviours. These analytic results are of both theoretical and practical importance and will be used in this work. For complexes situations, computational methods were developed (see interesting review in [28]) but they remain highly expensive for industrial applications.

3 Micro-macro decoupled computational homogenization

To overcome the computational cost due to the coupled homogenization method, some decoupled numerical approaches for homogenizing heterogeneous materials have been developed [112, 108, 109, 124, 10, 111, 110].

The principle of this method, which is related to the work of Terada and his co-workers [111], is the decoupling between the microscopic and macroscopic scales carried out by the *a priori* choice of a parametric homogenized law. The parameters of this law are adjusted to minimize the deviation with respect to a series of numerical tests (such as uniform tension, uniform compression and shearing tests) performed on a finite element approximation of the microscopic problem on the RVE. Once the parameters of the law have been optimized, it can be used to compute the deformation at the macroscopic level without solving many microscopic problems simultaneously. This obviously leads to the reduction of computational cost, compared for instance with the FE² strategy. The quality of the approximation depends of course on the choice of the form of the parametric homogenized law as well as on the strategy of choice of the set of tests (that we will call in the following the training set). In the following sections we describe the details of this method.

3.1 Selection of a parametrized homogenized law

As shown in the previous sections, the variables exchanged between the scales are the macro displacement gradient \tilde{H} and the average of the micro first Piola-Kirchhoff stress tensor \tilde{P} . In order to analyze the micro and macro problems separately, the macro-homogenized constitutive relationship inherent in the micro-structure and its mechanical behavior is approximated by an appropriate constitutive model. In simple situations, including the fiber reinforced matrix we consider, a possible way to design such constitutive model is to assume that the macroscopic material responses inherit the microscopic ones except for anisotropic behavior. Consequently, at this stage, and considering large elastic deformation, one has to select a parametrized elastic law, i.e., the macro-scale second Piola-Kirchhoff stress tensor

$$\tilde{\mathbf{S}}_h(\mathbf{p}, \tilde{\mathbf{H}}),$$

depending on a certain number of parameters

$$\mathbf{p} = (p_1, p_2, \dots, p_{n_{para}}).$$

In the hyperelastic framework, the elastic law derives from a potential $\tilde{W}_h(\mathbf{p}, \tilde{\mathbf{H}})$, in the sense that [74]

$$\tilde{\mathbf{S}}_h(\mathbf{p}, \tilde{\mathbf{H}}) = \frac{\partial \tilde{W}_h}{\partial \tilde{\mathbf{E}}}(\mathbf{p}, \tilde{\mathbf{H}}) = 2 \frac{\partial \tilde{W}_h}{\partial \tilde{\mathbf{C}}}(\mathbf{p}, \tilde{\mathbf{H}}),$$

where $\tilde{\mathbf{C}} = (\tilde{\mathbf{H}} + \mathbf{1})^T(\tilde{\mathbf{H}} + \mathbf{1})$ is the right Cauchy-Green deformation tensor and $\tilde{\mathbf{E}} = \frac{1}{2}(\tilde{\mathbf{C}} - \mathbf{1})$ the Green-Lagrange one. Often, the parametrized law is linear with respect to the coefficients, which means that it reads

$$\tilde{\mathbf{S}}_h(\mathbf{p}, \tilde{\mathbf{H}}) = \sum_{i=1}^{n_{para}} p_i \tilde{\mathbf{S}}_h^i(\mathbf{p}, \tilde{\mathbf{H}}), \quad (20)$$

or

$$\tilde{\mathbf{S}}_h(p, \tilde{\mathbf{H}}) = 2 \sum_{i=1}^{n_{para}} p_i \frac{\partial \tilde{W}_h^i}{\partial \tilde{\mathbf{C}}}(\tilde{\mathbf{H}}),$$

in the hyperelastic case, with $\tilde{\mathbf{S}}_h^i(\tilde{\mathbf{H}}) = 2 \frac{\partial \tilde{W}_h^i}{\partial \tilde{\mathbf{C}}}(\tilde{\mathbf{H}})$.

Even if this strategy can be applied in the case of fully parametric homogenized laws, as it is presented for instance in [126, 28] where interpolation functions are used to describe the homogenized potential, our objective in this study is to consider laws having a restricted number of parameters and allowing a low cost numerical modelling of the global structure.

3.2 Numerical material testing, definition of a training set

The idea is to “train” the law (i.e. to fit its parameters) on the response of the microstructure represented on the RVE for a representative set of solicitations. This is done by solving a finite element approximation of the BVP (9)-(10) for each solicitation. In our case, we select a set of n_{tests} gradients

$$\tilde{\mathbf{H}}^{[\alpha]}, \alpha = 1 \dots n_{test}.$$

Then, each gradient $\tilde{\mathbf{H}}^{[\alpha]}$ induces a finite element computation which allows in return to calculate the corresponding average of the first Piola-Kirchhoff tensor $\tilde{\mathbf{P}}^{[\alpha]}$ through the relation (17). In our case, the computation are performed using GetFEM [84] with Lagrange quadratic elements on the mesh represented on fig. 2 and a fifth-order cubature method with 15 points. This mesh has been selected after a numerical convergence test to ensure a good quality of the solution at a reasonable cost. Then, the second Piola-Kirchhoff tensor $\tilde{\mathbf{S}}^{[\alpha]}$ is obtained using

$$\tilde{\mathbf{S}}^{[\alpha]} = (\mathbf{1} + \tilde{\mathbf{H}}^{[\alpha]})^{-1} \tilde{\mathbf{P}}^{[\alpha]}. \quad (21)$$

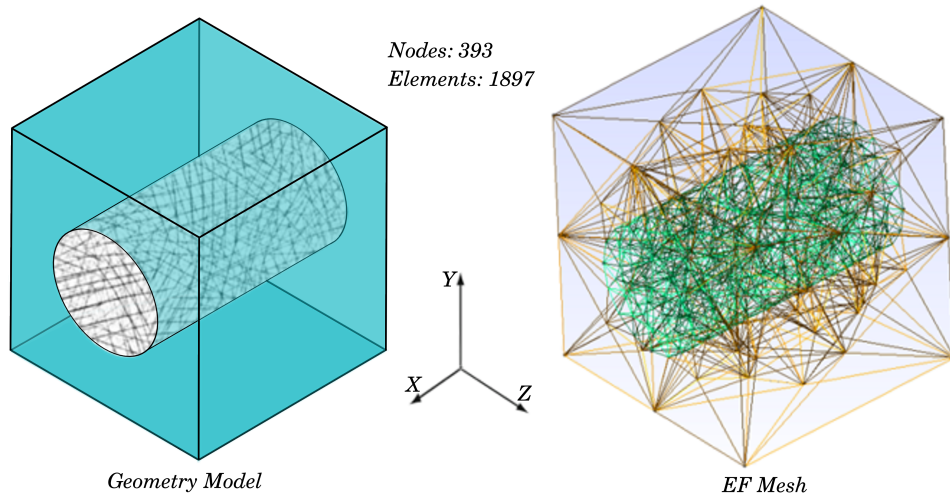


Figure 2: uni-directional fiber reinforced composite, geometry and finite element mesh

The tests are more or less expensive depending on the complexity of the microstructure represented in the RVE and the refinement of the finite element approximation. As far as we are concerned, the microstructure being relatively simple, the computations on the RVE are relatively cheap although on a three-dimensional RVE. In our case, the chosen unit cell model for the transverse isotropic material consists of two different materials: the matrix and the fiber. The matrix is assumed to be a cubic sample filling the three dimensional space in $[0, 1]^3$ with an inclusion of cylindrical shape. The FE mesh is generated taking into account the interface between the fiber

and the matrix, using tetrahedral elements. We employ, for the fibers and matrix, a fixed Poisson's ratio (ν_f, ν_m) and Young's modulus defined as

$$E_f = cE_m, \quad (22)$$

where c is the contrast constant and (f, m) are indices that refer to the fibers and the matrix, respectively.

Finally, we can apply to each solicitation a weight $w^{[\alpha]} > 0$, so that at the end of this step we obtain a training set made of triplets

$$\tilde{\mathbf{H}}^{[\alpha]}, \tilde{\mathbf{S}}^{[\alpha]}, w^{[\alpha]}, \alpha = 1 \dots n_{test}.$$

For the identification of the coefficients of the chosen potential to be as representative as possible, it is important to give a sufficiently varied panel of solicitations. We apply 6 basic patterns (and some combinations) of macroscopic strains by imposing displacement gradient $\tilde{\mathbf{H}}$, introduced in table 1. Here, h and $(\varepsilon_1, \varepsilon_2, \varepsilon_3)$ are the specified and unspecified components of the macro-scale displacement gradient $\tilde{\mathbf{H}}_i (i = 1, \dots, 6)$, respectively. We choose the limiting strain level such that $h \in [-0.5, 0.5]$. The values of $(\varepsilon_1, \varepsilon_2, \varepsilon_3)$ are fixed to $(0, 0, 0)$ in the compressible case and are determined to satisfy the following volume conservation condition in the incompressible case:

$$\det(\tilde{\mathbf{H}}(X) + \mathbb{1}) = 1.$$

Pattern-1: Uniaxial tension in the direction of x $\tilde{\mathbf{H}}_1 = \begin{pmatrix} h & 0 & 0 \\ 0 & \varepsilon_2 & 0 \\ 0 & 0 & \varepsilon_3 \end{pmatrix}$	Pattern-4: xy shear $\tilde{\mathbf{H}}_4 = \begin{pmatrix} \varepsilon_1 & h & 0 \\ h & \varepsilon_2 & 0 \\ 0 & 0 & \varepsilon_3 \end{pmatrix}$
Pattern-2: Uniaxial tension in the direction of y $\tilde{\mathbf{H}}_2 = \begin{pmatrix} \varepsilon_1 & 0 & 0 \\ 0 & h & 0 \\ 0 & 0 & \varepsilon_3 \end{pmatrix}$	Pattern-5: xz shear $\tilde{\mathbf{H}}_5 = \begin{pmatrix} \varepsilon_1 & 0 & h \\ 0 & \varepsilon_2 & 0 \\ h & 0 & \varepsilon_3 \end{pmatrix}$
Pattern-3: Uniaxial tension in the direction of z $\tilde{\mathbf{H}}_3 = \begin{pmatrix} \varepsilon_1 & 0 & 0 \\ 0 & \varepsilon_2 & 0 \\ 0 & 0 & h \end{pmatrix}$	Pattern-6: yz shear $\tilde{\mathbf{H}}_6 = \begin{pmatrix} \varepsilon_1 & 0 & 0 \\ 0 & \varepsilon_2 & h \\ 0 & h & \varepsilon_3 \end{pmatrix}$

Table 1: Deformation patterns on the RVE

3.3 Identification of the homogenized law

Once the training set has been determined, the identification of coefficients of the homogenized law $\tilde{S}_h(\mathbf{p}, \tilde{\mathbf{H}}^{[\alpha]})$ is performed using a least squares optimization, by minimizing the following quantity:

$$J(\mathbf{p}) = \frac{1}{2\omega_*} \sum_{\alpha=1}^{n_{test}} w^{[\alpha]} \frac{\|\tilde{S}_h(\mathbf{p}, \tilde{\mathbf{H}}^{[\alpha]}) - \tilde{\mathbf{S}}^{[\alpha]}\|^2}{\|\tilde{\mathbf{S}}^{[\alpha]}\|^2}, \quad (23)$$

with $\omega_* = \sum_{\beta=1}^{n_{test}} w^{[\beta]}$ the sum of the weights, and $\|\cdot\|$ the Frobenius norm for second order tensors.

This minimization can be performed with or without constraints on the values of the parameters. For instance, most constitutive laws have coefficients that are intended to remain positive and ensure interesting properties (such as polyconvexity) with positive coefficients [98, 96]. In this case, constraining the coefficients to remain positive can avoid modelling problems (such as spurious zero energy deformations).

In the specific case where the homogenized law $\tilde{\mathbf{S}}_h(\mathbf{p}, \tilde{\mathbf{H}}^{[\alpha]})$ is linear with respect to its coefficients, i.e. in the form (20), and if no constraints on the parameters are considered, the minimization of (23) leads to the following linear system:

$$A \begin{pmatrix} p_1 \\ \vdots \\ p_{n_{para}} \end{pmatrix} = L, \quad \text{with} \quad \begin{cases} A_{ll} = \frac{1}{\omega_*} \sum_{j=1}^{n_{test}} w^{[j]} \frac{1}{\|\tilde{\mathbf{S}}^{[j]}\|^2} \tilde{\mathbf{S}}_h^l : \tilde{\mathbf{S}}_h^l, \\ A_{il} = \frac{1}{2\omega_*} \sum_{j=1}^{n_{test}} w^{[j]} \frac{1}{\|\tilde{\mathbf{S}}^{[j]}\|^2} \tilde{\mathbf{S}}_h^l : \tilde{\mathbf{S}}_h^i \quad \forall i \neq l, \\ L_l = \frac{-1}{\omega_*} \sum_{j=1}^{n_{test}} w^{[j]} \frac{1}{\|\tilde{\mathbf{S}}^{[j]}\|^2} \tilde{\mathbf{S}}_h^l : \tilde{\mathbf{S}}^{[j]}. \end{cases}$$

Of course, the last step of the method, once the homogenized law is identified, is to solve the macro-scale BVP using this constitutive law, generally approximated also by a finite element method. Moreover, since the homogenized law is approximated within the framework of a two-variables boundary value problem derived from a homogenization theory, the macro response obtained using this model can be regarded as approximating the data of the micro problem at each material point.

3.4 Example of the NeoHookean hyperelastic law for both fiber and matrix

The validity of the micro-macro computational decoupled homogenization procedure developed in section 3 is investigated by comparison of its predictions with an explicit expression for the effective behaviour of fiber composites [40, 72] developed initially for an incompressible transverse isotropic hyperelastic behaviour (i.e. when both $D_{1,m}$ and $D_{1,f}$ goes to infinity) in [13]. For computational reasons, the fiber and the matrix of the RVE micro-structure are represented by a nearly incompressible NeoHookean potential

$$W_{NH,i} = C_{01,i}(\underline{I}_1 - 3) + D_{1,i}(J - 1)^2 \quad (i = f, m), \quad (24)$$

where $J = \det(\mathbf{F})$ is the Jacobian of the deformation, $\underline{I}_1 = \text{tr}(\underline{\mathbf{C}})$ is the invariant of the isochoric Cauchy-Green strain tensor $\underline{\mathbf{C}} = \underline{\mathbf{F}}^T \cdot \underline{\mathbf{F}} = J^{-2/3} \mathbf{F}^T \cdot \mathbf{F} = I_3^{-1/3} \mathbf{C}$ with $\underline{\mathbf{F}} = J^{-1/3} \mathbf{F}$ and $I_3 = \det(\mathbf{C}) = J^2$, $C_{01,i}$ and $D_{1,i}$ are given coefficients that can be related to Young's modulus and Poisson's ratio by the formula

$$C_{01,i} = \frac{E_i}{4(1 + \nu_i)}, \quad D_{1,i} = \frac{E_i}{6(1 - 2\nu_i)}, \quad (25)$$

where we take E_i and ν_i as the Young modulus and the Poisson coefficients of the fiber and the matrix materials with $E_f = 203 \text{ GPa}$ and $E_m = E_f/c$, with c the contrast.

The strain energy decomposition defined by (24) governs a slightly compressible material behaviour. If the material behaviour is incompressible, i.e. the coefficients $D_{1,i} \rightarrow \infty$, that energy corresponds to the NeoHookean potential corresponding to the simplest phenomenological and molecular constitutive model function of rubber like materials [114]. However, its capability to predict experimental data is poor especially at high values of deformation. Nevertheless, the NeoHookean strain energy model is essentially to deduce analytic solutions of boundary-value problems [74] within the framework of finite elasticity.

The explicit expression for the effective behaviour of fiber/matrix RVE composite is developed by DeBotton and his co-workers in [13] exploiting the analytical homogenized method [40, 72]. The resulting homogenized law is an incompressible transversely isotropic NeoHookean hyperelastic model [13]. An extension to a nearly incompressible behaviour will be exploited in this work

$$\tilde{W}_h = \frac{\tilde{\mu}}{2}(\underline{I}_1 - 3) + \frac{\bar{\mu} - \tilde{\mu}}{2}\left(\underline{I}_4 + \frac{2}{\sqrt{\underline{I}_4}} - 3\right) + D(J - 1)^2, \quad (26)$$

where $\underline{I}_4 = \mathbf{A} \cdot \tilde{\mathbf{C}} \mathbf{A}$, \mathbf{A} is the unit vector along the fiber in the reference configuration, and the coefficients $\tilde{\mu}$ and $\bar{\mu}$ are scalar-valued material parameters given by

$$\begin{aligned} \tilde{\mu} &= \mu_m \frac{(1 + c^f)\mu_f + (1 - c^f)\mu_m}{(1 - c^f)\mu_f + (1 + c^f)\mu_m}, \\ \bar{\mu} &= \mu_f c^f + \mu_m c^m, \end{aligned} \quad (27)$$

with $0 < c^f < 1$ the volume fraction of fiber, $c^m = 1 - c^f$ the volume of fraction of matrix and μ_f, μ_m the infinitesimal shear modulus of the fiber and matrix, respectively.

For transversely hyperelastic behaviour, the decomposition (26) was first adopted in [120] and [42] and is also adopted by the quasi-totality of commercial and open-source finite element codes.

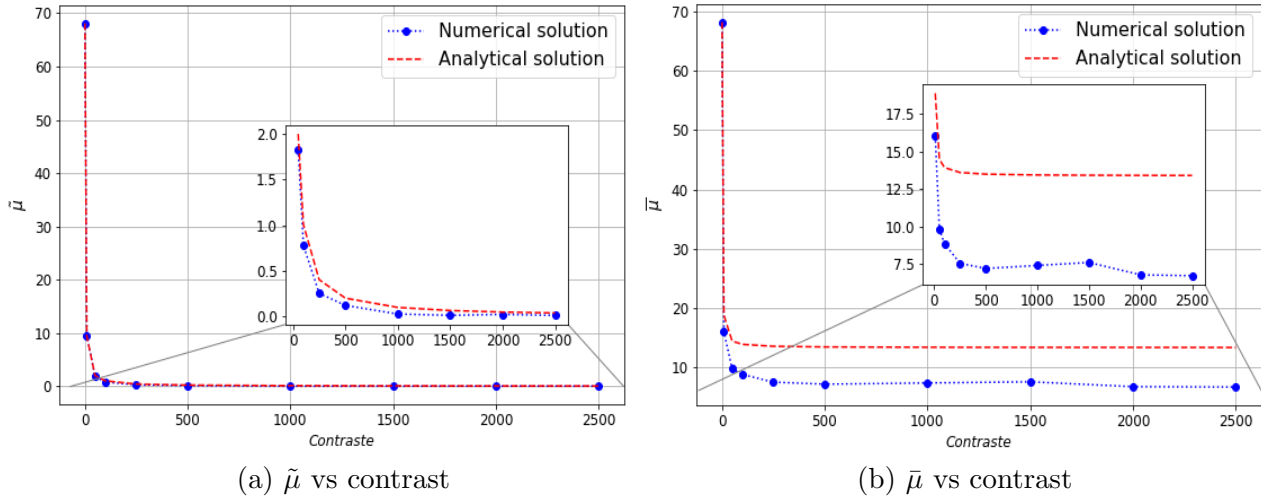


Figure 3: Identification of the coefficients $\tilde{\mu}$ and $\bar{\mu}$ for Poisson coefficient $\nu = 0.49$ and for contrast $c \in [1, 2500]$.

Please note that the value $c = 1$ is utilized to validate the implementation of the methodology.

The test are performed with $\nu = \nu_f = \nu_m$ varying from 0.49 to 0.4999 and with $c^f = 0.196$. No specific numerical treatment has been used for the finite element approximation of the quasi-incompressible matrix apart the use of quadratic elements. We verified the absence of locking phenomenon by checking the regularity of the deformation with respect to the Poisson ratio when it approaches 0.5. We perform the identification of the parameters of the homogenized law (26) with a training set composed of 50 experiments for each of the 6 simple patterns of table 1 and also for 9 additional patterns which are combinations of the simple ones as $\tilde{\mathbf{H}}_i + \tilde{\mathbf{H}}_j$ for $i \in \{1, 2, 3\}$ and $j \in \{4, 5, 6\}$. The 50 experiments are regularly distributed in a logarithmic scale up to a deformation of 30% and we use uniform weights ($\omega^{[\alpha]} = 1$ in (23)). Then, we compare the results with the theoretical values (27).

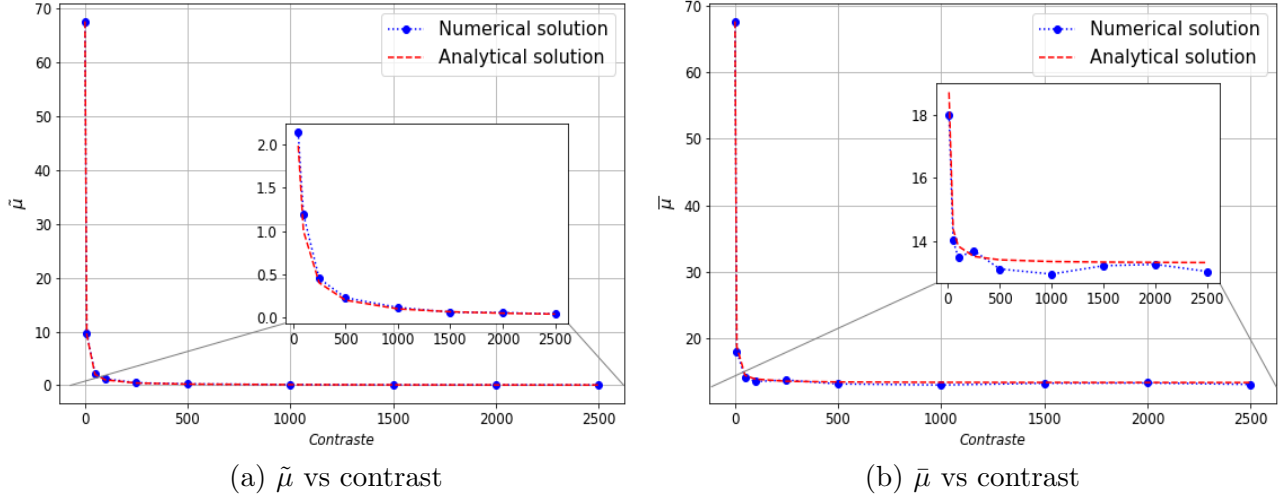


Figure 4: Identification of the coefficients $\tilde{\mu}$ and $\bar{\mu}$ for Poisson coefficient $\nu = 0.4999$ and for contrast $c \in [1, 2500]$.

The result of the identification, presented on fig. 3 for a Poisson coefficient $\nu = \nu_f = \nu_m = 0.49$, shows a relatively good agreement between the identified value of $\tilde{\mu}$ and its theoretical value. On the contrary, there is a significant difference for $\bar{\mu}$. This a priori means that $\nu = 0.49$ is not close enough to the incompressibility. The differences are much smaller on fig. 4 for a Poisson coefficient $\nu = \nu_f = \nu_m = 0.4999$ closer to the incompressibility limit for which the theoretical values (27) are valid. Overall, these numerical experiments show that the identification based on a training set allows to identify the homogenized law with a good accuracy.

4 Local error

In the case of the previous section, the homogenized law has been identified exactly and therefore the decoupling does not induce additional approximation. In the general case where this identification cannot be done exactly, the form of the chosen homogenized law corresponds to an additional approximation. One way to measure the approximation made once the identification is done on a particular training set, is to compute the local error between the homogenized law and the average of second Piola-Kirchhoff tensor calculated on the RVE. For this purpose, the following local error is introduced:

$$\text{Err}(\tilde{\mathbf{H}}^{[\alpha]}) = \frac{\left\| \tilde{\mathbf{S}}_h(p, \tilde{H}^{[\alpha]}) - \tilde{\mathbf{S}}^{[\alpha]} \right\|}{\left\| \tilde{\mathbf{S}}^{[\alpha]} \right\|}.$$

This error must be zero for any $\tilde{H}^{[\alpha]}$ in the case of exact decoupling. In the following sections, we present numerical studies of this local error for different choices of homogenized laws.

For the rest of this study, the fiber is represented by a Saint-Venant Kirchhoff hyperelastic law for which the potential reads

$$\tilde{W}_{SVK} = \frac{\lambda_f}{2} [\text{tr}(\mathbf{E})]^2 + \mu_f \text{tr}(\mathbf{E}^2), \quad (28)$$

with $\lambda_f = \frac{E_f \nu_f}{(1+\nu_f)(1-2\nu_f)}$ and $\mu_f = \frac{E_f}{2(1+\nu_f)}$ and $E_f = 203\text{GPa}$, $\nu_f = 0.3$. This model only extends the geometrically linear Hooke elastic material model to the geometrically nonlinear region as has

been presented in [117]. Even though it appears to have deficiencies in large strain areas, it has since attracted a lot of interest [3] [4] [95].

The matrix is represented by a compressible Mooney-Rivlin hyperelastic potential

$$W_{MR} = c_{01,m}(\underline{I}_1 - 3) + c_{10,m}(\underline{I}_2 - 3) + d_{1,m}(J - 1)^2, \quad (29)$$

with $c_{01,i} = \frac{E_m}{4(1+\nu_m)}$, $c_{10,i} = 0.15c_{01,i}$, $d_{1,i} = \frac{E_m}{6(1-2\nu_m)}$ and $\nu_m = 0.49$ and for different values of E_m corresponding to different contrasts $c = \frac{E_f}{E_m}$.

The incompressible version of the hyperelastic model (29) was first published by Melvin Mooney in [62] and Ronald Rivlin later defined it in terms of invariants [88]. It is also to be noted that the Mooney-Rivlin (MR) model is an extension of the NeoHookean model that attempts to improve the accuracy by including a linear dependence on the second invariant \underline{I}_2 of the strain energy [45].

In both of the homogenized potentials below, we will study the difference between the local error results of the identified coefficients of the homogenized law using the Sequential Least Squares Programming (SLSQP) method. In this study, we will impose the constraints on positivity of the coefficients to preserve the consistency of the law and the training set is still build using 50 experiments for each of the 6 simple patterns of table 1 and also for 9 additional patterns as described in section 3.4.

4.1 Slightly compressible hyperelastic model : original decoupled Kalske's transversely isotropic law

One way to develop hyperelastic models is to extend existing incompressible hyperelastic models to compressible behaviour. This is done by assuming an additive split of the strain energy into two parts: a volumetric W_{vol} strain energy depending on volume change invariant J and a isochoric (deviatoric) W_{isc} one function of isochoric strain $\tilde{\underline{\mathbf{C}}}$. This is inspiring by the multiplicative decomposition of the deformation gradient introduced in [26]:

$$\tilde{W}_h(\tilde{\underline{\mathbf{C}}}, J; \mathbf{A}) = W_{vol}(J) + W_{isc}(\tilde{\underline{\mathbf{C}}}; \mathbf{A}), \quad (30)$$

This decomposition (30), originally proposed for isotropic behaviour when the hydrostatic Cauchy stress is a function only of J [73], should verify some constraint. For incompressible behaviour $J = 1$, the strain energy $\tilde{W}_h(J = 1, \tilde{\underline{\mathbf{C}}}; \mathbf{A})$ should recover a known incompressible hyperelastic model with the constraint $W_{vol}(J = 1) = 0$ and depend on (I_4, I_5) invariant [51]. In the case of small deformations, the strain energy should be compatible with the linear elasticity theory. Notice that the split into bulk and deviatoric strain energies has the convenience of facilitating material identification through bulk and shear responses. This decoupled sum of strain energies is also crucial for improving the finite element implementation to avoid numerical locking problems for nearly incompressible analysis [103]. Attention should be made for material behaviour that is not nearly incompressible, the decomposition leads to unphysical responses [15].

The key question addressed here is if the decomposition (30) is also available for anisotropic behaviour. For the moment, the strain energy decoupled form is adopted.

In this work, the homogenized material is modelled by a hyperelastic potential as a sum of a volumetric energy function of the Jacobian W_{vol} which is the response of the material to volume changes and an isochoric energy function W_{isc} depends only on the distortional part of the deformation which can be divided into W_{iso} and W_{aniso} for the energy contributions of the matrix as domineering ground substance and and the fibers, respectively:

$$W_{vol} = D(J - 1)^2, \quad (31)$$

$$W_{isc} = W_{iso}(\underline{I}_1, \underline{I}_2) + W_{aniso}(\underline{I}_4, \underline{I}_5; \mathbf{A}), \quad (32)$$

where the isochoric invariants of $\tilde{\mathbf{C}}$ are defined as $\underline{I}_2 = \frac{1}{2}(\text{tr}^2(\tilde{\mathbf{C}}) - \text{tr}(\tilde{\mathbf{C}}^2))$, for the first layer $\underline{I}_4 = \mathbf{A} \cdot \tilde{\mathbf{C}} \mathbf{A}$, $\underline{I}_5 = \mathbf{A} \cdot \tilde{\mathbf{C}}^2 \mathbf{A}$ and \mathbf{A} still being a unit vector along the layer fiber.

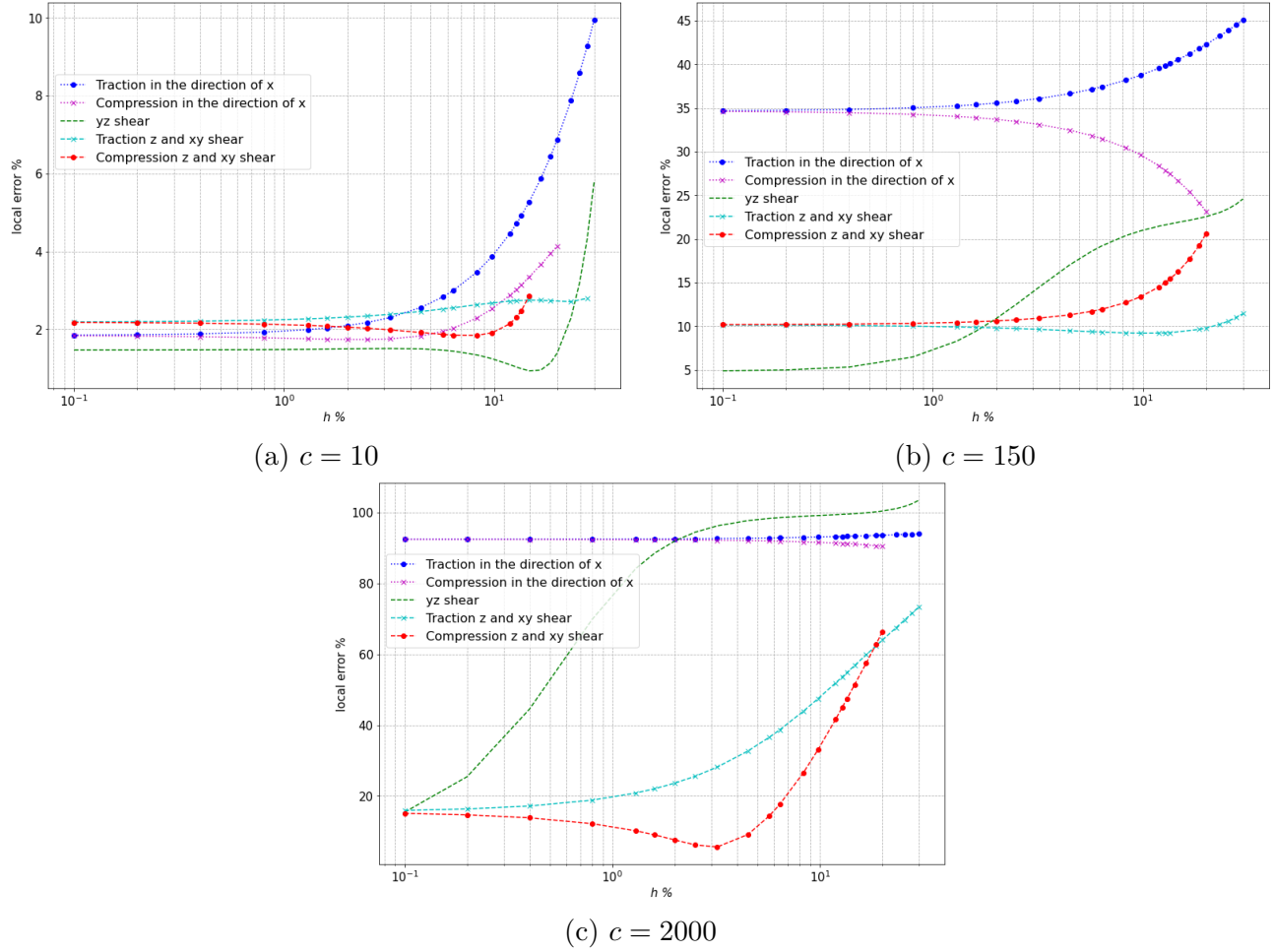


Figure 5: Local error for Kaliske's transverse isotropic law with respect to the deformation and three different contrasts

The isochoric strain energy density function of Kaliske, as presented in [49] and in particular used in a similar context for periodic unidirectional composite layer in [111], reduces to

$$W_{iso} = \sum_{i=1}^3 a_i (\underline{I}_1 - 3)^i + \sum_{j=1}^3 b_j (\underline{I}_2 - 3)^j, \quad (33)$$

$$W_{aniso} = \sum_{k=2}^6 c_k (\underline{I}_4 - 1)^k + \sum_{l=2}^6 d_l (\underline{I}_5 - 1)^l. \quad (34)$$

The tests are performed for a range of deformations up to 30% and for three different contrast values ($c = 10$, $c = 150$ and $c = 2000$).

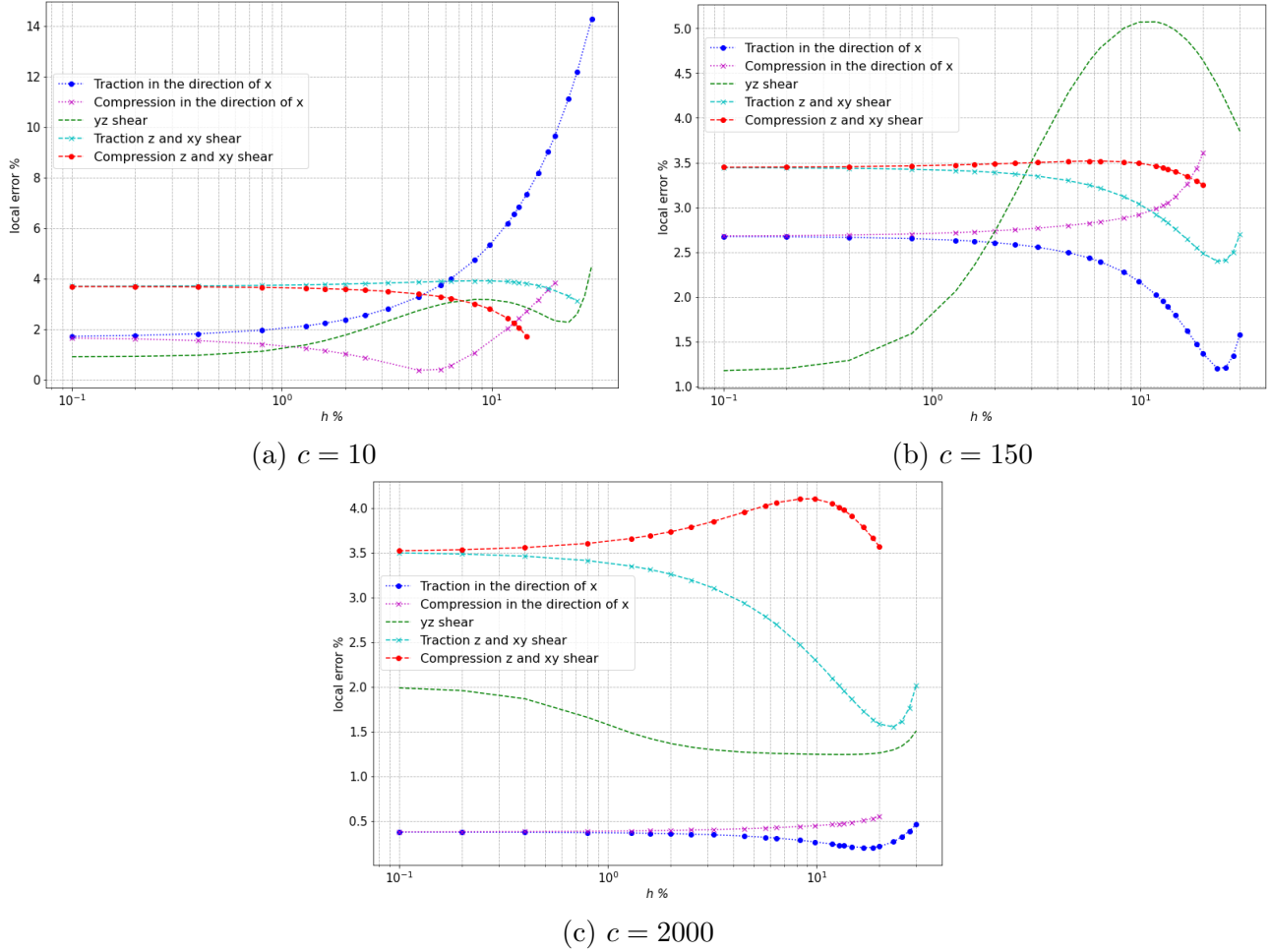


Figure 6: Local error for the variant of Kaliske's transverse isotropic law with respect to the deformation and three different contrasts

The local errors shown in fig. 5 are quite large, except for the lowest contrast value ($c = 10$) and even for small deformations. Our interpretation of this very poor approximation for a high value of the contrast is that isochoric invariants \underline{I}_1 , \underline{I}_2 , and especially \underline{I}_4 and \underline{I}_5 being insensitive to uniform compression, the only term in Kaliske's law which is responsible for the response to a uniform compression is the volumetric one. This means in particular that a uniform compression result in an isotropic response, even for a high value of the contrast, which is not the expected behavior. Our conclusion is that Kaliske's law cannot be used for a high value of contrast in the context of our study (nearly incompressible matrix and compressible fiber) and we therefore propose a variant for the anisotropic part in the next section.

The analysis done below is corroborated by theoretical and numerical works. In fact, it seems that the decomposition was generalized to anisotropic behaviour [120] and [41] without theoretical, numerical and experimental analysis. Firstly, it is shown that the fibers play no role for a cube or a sphere under hydrostatic tension [37] [68] [118] [71] [29] [79]. Secondly, the decomposition is not compatible with anisotropic linear elastic theory [94] [20] [78] [63] as it is expected to be for any nonlinear theory [82].

4.2 Modified slightly compressible hyperelastic model : Variant of Kálik's transverse isotropic law

Following the conclusion of the previous section that the deficiency of Kálik's law comes from the fact that isochoric invariants are used even for the anisotropic part, which does not fit well with the numerical experiments on the RVE, we propose a variant of this law replacing the strain energy density function (34) for the anisotropic part by the following one which uses standard invariants:

$$W_{aniso} = \sum_{k=2}^6 c_k (I_4 - 1)^k + \sum_{l=2}^6 d_l (I_5 - 1)^l. \quad (35)$$

This enrichment of the anisotropic part of hyperelastic model (34) was first proposed in [71] [119] and its prediction capability was attested in [70]. Notice that another enrichment of the anisotropic part of hyperelastic model (34) was proposed in [29] by assuming that the hydrostatic Cauchy stress is a function of volume change and anisotropic invariants. There are also other theoretical contributions to overcome the drawback of the volumetric/deviatoric strain energy decomposition performed in [78][63].

The corresponding local errors can be seen in fig. 6. The error level is slightly higher for the contrast ($c = 10$) for moderate deformations. Along with this, there is a huge improvement of the approximation for high values of contrast, with less than 5% of error and no degradation for large deformations.

In the context of the rest of our study, we will focus on a high value of contrast ($c = 2000$) compatible with a couple of materials such as rubber and steel. Consequently, we will consider only this variant of Kálik's law instead of the original one.

4.3 Bonet's transverse isotropic law

An alternative approach to avoid the drawback of the volumetric/isochoric multiplicative decomposition of the deformation gradient can be described well by the fiber-reinforced continuum mechanics theory of [17, 105]. To do this, a phenomenological approach is usually adopted and the anisotropic compressible hyperelastic potential is expressed in various functional forms such as a series of polynomials or exponentials within the framework of the invariant theory [97, 99, 8, 75, 76].

In this work, Bonet's transverse isotropic potential [7] is considered, which is a combination of an isotropic strain energy density function W_{iso} characterising the rubber type of materials in the large strain (NeoHookean potential), and a transverse one W_{trn} defined as follows:

$$\tilde{W}_h = W_{iso} + W_{trn}, \quad (36)$$

$$W_{iso} = \mu_{iso} \left(\frac{1}{2} (I_1 - 3) - \ln(J) \right) + \frac{\lambda_{iso}}{2} (\ln(J))^2, \quad (37)$$

$$W_{trn} = (a_{tr} + b_{tr} \ln(J) + c_{tr} (I_4 - 1)) (I_4 - 1) - \left(\frac{1}{2} a_{tr} + d_{tr} \ln(J) \right) (I_5 - 1), \quad (38)$$

where $I_1 = \text{tr}(\tilde{\mathbf{C}})$, $I_4 = \mathbf{A} \cdot \tilde{\mathbf{C}} \mathbf{A}$, $I_5 = \mathbf{A} \cdot \tilde{\mathbf{C}}^2 \mathbf{A}$, and \mathbf{A} still being a unit vector along the fiber in the reference configuration. Note that we consider an improved version of [69] instead of the original one in [7] where $b_{tr} \ln(J)$ replaces $b_{tr} (I_1 - 3)$ and $d_{tr} \ln(J) (I_5 - 1)$ is added to improve the identification of the homogenized material parameters [51]. This strain energy decomposition (36) into isotropic (37) and anisotropic (38) parts was suggested in [42] to simplify the model complexity and to facilitate model's parameters experimental identification.

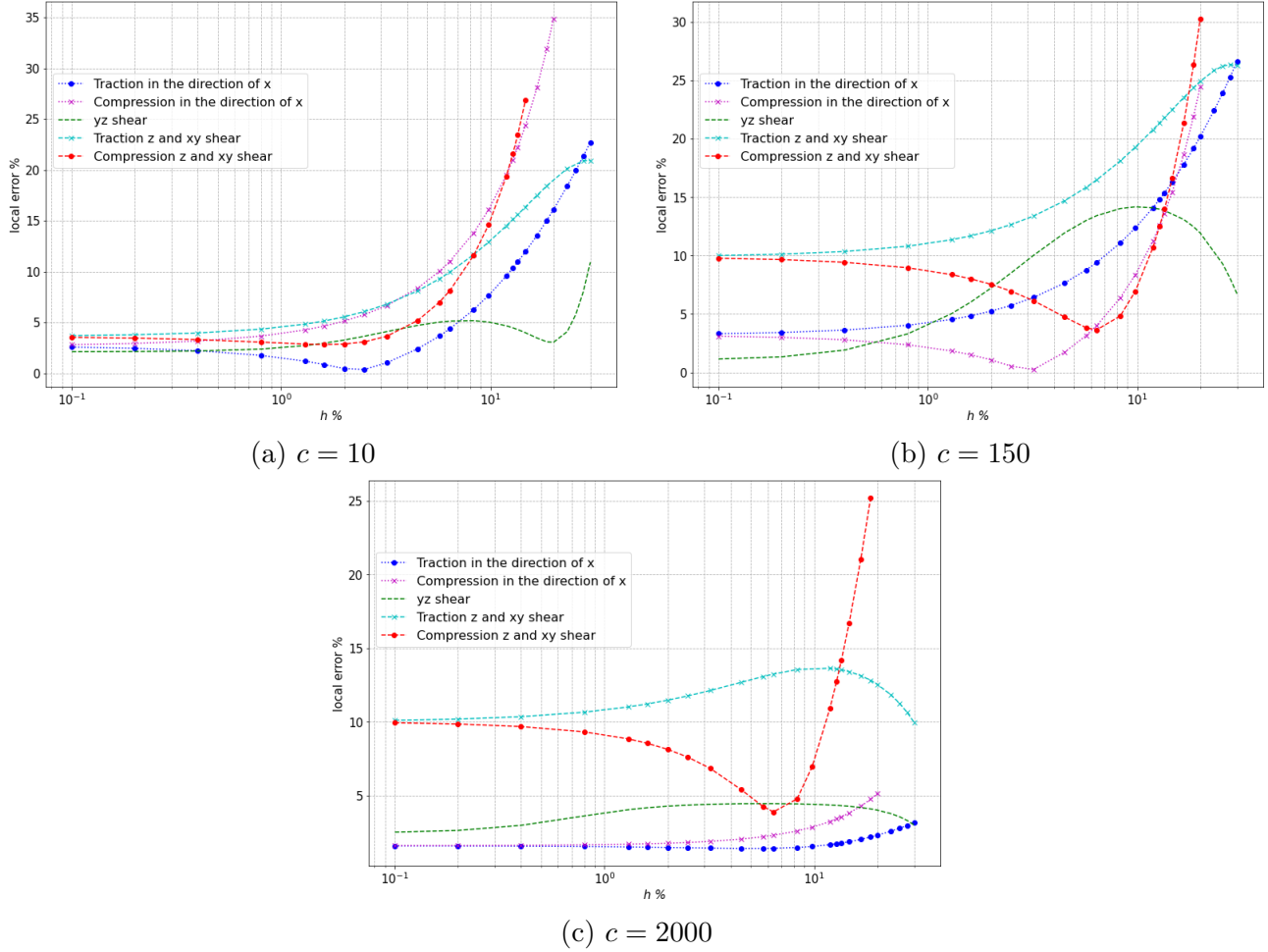


Figure 7: Local error for Bonet’s transverse isotropic law with respect to the deformation and three different contrasts

This hyperelastic model decoupled assumption is motivated by physical arguments coming from the fiber and matrix behaviour which are assumed isotropic. At small deformation, the fibres, which are more rigid than the matrix, are less active and then the behaviour is governed by isotropic strain energy part. At large deformation, the fibres come into play (it is their role), the anisotropic strain energy part pilots the mechanical behaviour.

The numerical tests are identical to those performed for Kaliske’s traditional decoupled model in the previous section. After identification, the local errors are shown in fig. 7 for three selected deformation patterns of table 1 and two additional mixed ones. A local error less than 5% is only obtained for a low contrast ($c = 10$) and for small deformations (less than 1%). Moreover, for that contrast, there is an important degradation of the approximation for large deformations. For a high contrast ($c = 150$ and $c=2000$) the maximal local error is about 10% for moderate deformations. The degradation for large deformations is less important, except for the last mixed deformation pattern (compression z and xy shear).

5 Correction method

5.1 Test on a complete fiber reinforced layer

In order to test the relevance of the homogenization procedure, we make a comparative test between the deformation of a fully meshed fiber reinforced layer and of the same structure using the homogenized law. The tests are conducted with quadratic Lagrange elements in our finite element library GetFEM++ [84] (using a fifth-order cubature method with 15 points).

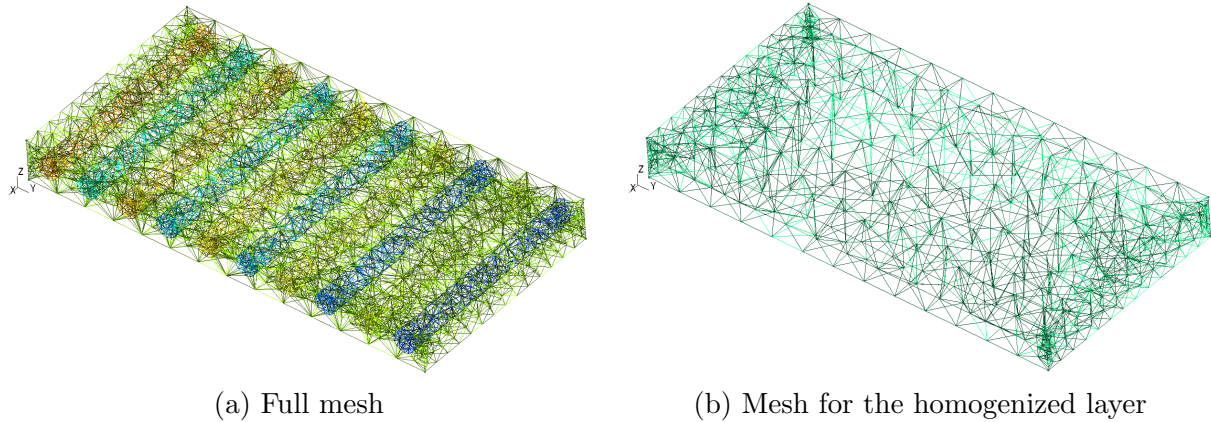


Figure 8: Meshes for the fiber reinforced layer: (a) mesh of the fibers and matrix for the full computation and (b) simpler mesh for the homogenized law

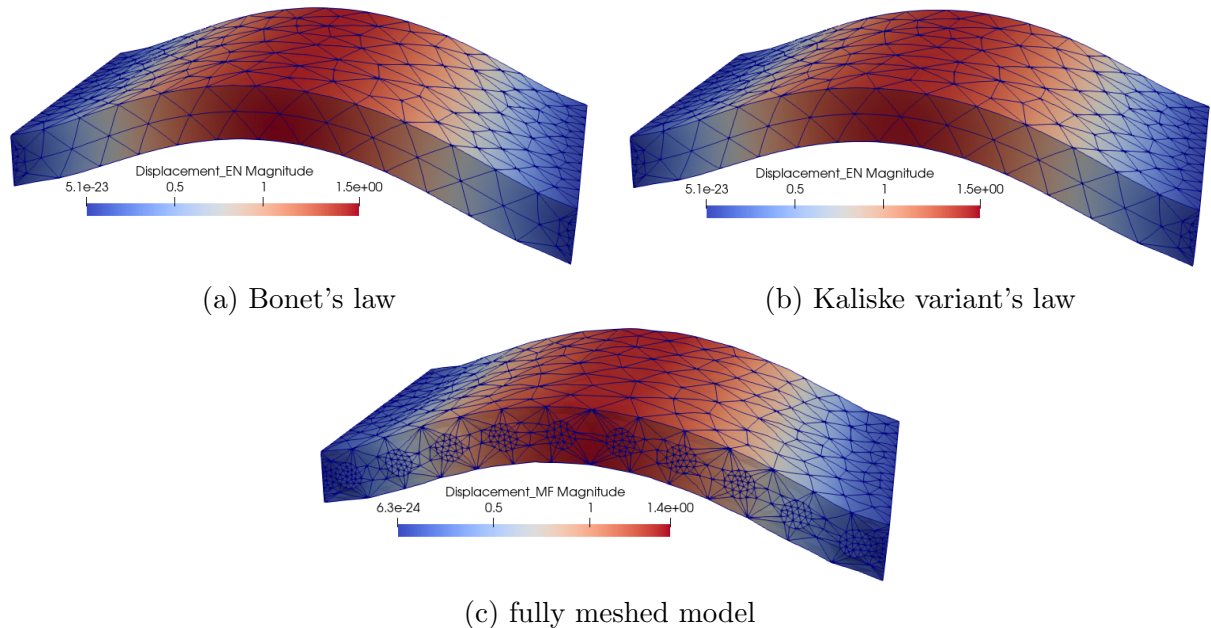


Figure 9: Comparison of the deformation of the layer obtained after homogenization with Bonets's law (a), Kaliske variant's law (b) and without homogenization with the fully meshed model (c).

Denoting $\tilde{\mathbf{U}}_e$ the approximated displacement of the complete FE model and $\tilde{\mathbf{U}}_h$ the one which

uses the homogenized law, we consider the following relative global error

$$\text{Err} = \frac{\|\tilde{\mathbf{U}}_h - \tilde{\mathbf{U}}_e\|}{\|\tilde{\mathbf{U}}_e\|}, \quad \text{where } \|\tilde{\mathbf{U}}_e\| = \left(\int_{\tilde{\mathcal{B}}_0} |\tilde{\mathbf{U}}_e|^2 d\tilde{V} \right)^{1/2}.$$

Of course, this error reflects several approximations: the finite element one, the homogenization principle itself and finally, what's interest to us, the approximation due to the choice of parametric constitutive law in the decoupled homogenization.

The meshes used for the heterogenous computation and the homogenized one are represented in fig. 8. These meshes has been selected after a convergence test and ensure a good quality of the solution and, as far as we checked, no numerical locking effects. The deformation obtained for the fully meshed model, the homogenized one using Bonet's law and the homogenized one using Kaliske variant's law can be seen in fig. 9 for comparison. A zoom of a superposition of the three deformations is also presented in fig. 10 where it is possible to see that Kaliske variant's law allow a slightly better approximation than Bonet's law.

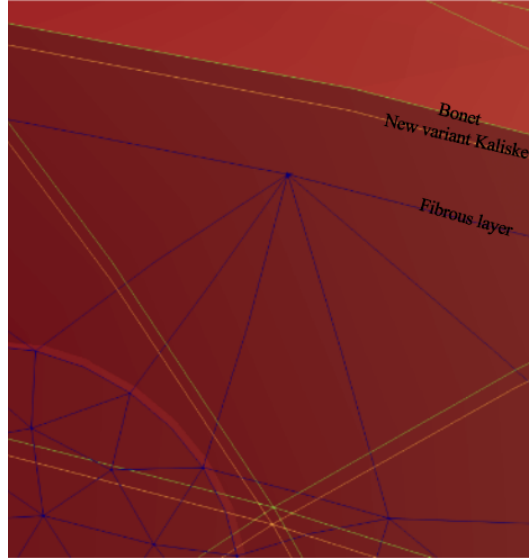


Figure 10: Zoom of the superposition of the deformation for the three situations: full model, homogenized one with Bonet's law, homogenized one with Kaliske variant's law

5.2 Correction method

In order to improve the quality of the approximation provided by the decoupled method, we propose an iterative method whose objective is to adapt the optimization of the homogenized law to the considered structural computation at a much lower computational cost than the FE² method [22].

The reference configuration $\tilde{\mathcal{B}}_0$ of the macroscopic structure is divided into a certain number of parallelepipedic element volumes

$$\mathcal{B}_p^{[\alpha]}, \quad \alpha = 1 \dots n_{vol},$$

distributed all over the structure. As far as possible, the chosen volumes should be representative of the micro-structure. However, this does not seem mandatory and their number should not be

excessive in order not to penalize the calculation time. These volumes can also be placed in zones of interest of the considered structure. The proposed method can then be divided into the following steps:

1. Determine a training set by the choice of $\tilde{\mathbf{H}}^{[\alpha]}$, $\alpha = 1 \dots n_{test}$ deformation patterns and the computation of the corresponding $\tilde{\mathbf{S}}^{[\alpha]}$ by n_{test} computations on the micro-scale BVP. Choose a set of weights $w^{[\alpha]}$, $\alpha = 1 \dots n_{test}$.
2. Perform the identification of the coefficients of the homogenized law with the considered training set by minimization of (23).
3. Compute a finite element approximation \mathbf{u}^h of the displacement of the structure by solving numerically the decoupled macro-scale BVP using the homogenized law.
4. On each volume $\mathcal{B}_p^{[\alpha]}$, compute numerically the average of deformation

$$\tilde{\mathbf{H}}_p^{[\alpha]} = \frac{1}{|\mathcal{B}_p^{[\alpha]}|} \int_{\mathcal{B}_p^{[\alpha]}} \nabla \mathbf{u}^h d\mathbf{V},$$

and the corresponding average of second Piola-Kirchhoff tensor $\tilde{\mathbf{S}}_p^{[\alpha]}$ by n_{vol} computations on the micro-scale BVP.

5. Loop to step 2 with the initial training set completed by $\tilde{\mathbf{H}}_p^{[\alpha]}$, $\tilde{\mathbf{S}}_p^{[\alpha]}$, $\alpha = 1 \dots n_{vol}$ with some chosen weights $w_p^{[\alpha]}$, $\alpha = 1 \dots n_{vol}$.

In order to test the correction method, we use different weights $\omega = 1, 10, 100$ for the deformation test flexion with two fixed edges with a deformation force density of 2MPa and in our case the number of parallelepipedic element volumes of the layer is $n_{vol} = 50$ (the weights for the initial training set are kept uniform to the value $\omega = 1$),

Fig. 11 shows the error distribution between the heterogeneous reference solution and the homogenized problem solution before and after a correction step using Bonet's potential. The global error and the local errors on the element volumes of the layer are reported in table 6. We can see a significant improvement from the first iteration for all considered weights, whether on the global error or on the local errors. In the considered case, the weight of $w_p^{[\alpha]} = 10$ for the layer volumes seems to be the best compromise, a weight of $w_p^{[\alpha]} = 100$ degrades a little the results. We can also notice that the next iterations (2 and 3) do not allow to improve the errors, either global or local. These errors remain very close or even with a slight degradation. We can conclude that the main part of the correction in this case is done at the first iteration of correction.

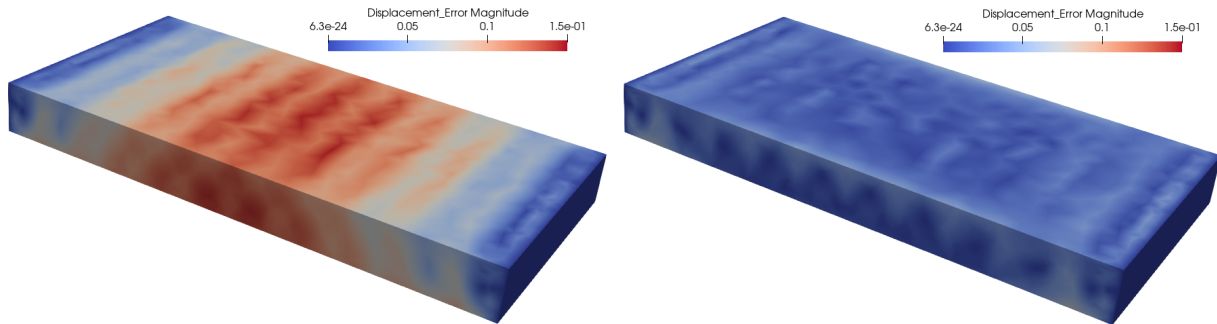


Figure 11: Error distribution before correction for Bonet's potential (left) and after correction (right)

	Before correction	weight	After correction		
			1 iteration	2 iterations	3 iterations
Global error	$Err_g = 10.13\%$	1	$Err_g = 4.33\%$	$Err_g = 4.75\%$	$Err_g = 4.72\%$
		10	$Err_g = 1.65\%$	$Err_g = 1.8\%$	$Err_g = 1.77\%$
		100	$Err_g = 1.81\%$	$Err_g = 1.67\%$	$Err_g = 1.68\%$
Average local error on layer volume elements	$Err_{al} = 18.31\%$	1	$Err_{al} = 12.48\%$	$Err_{al} = 12.77\%$	$Err_{al} = 12.74\%$
		10	$Err_{al} = 10.19\%$	$Err_{al} = 10.07\%$	$Err_{al} = 10.09\%$
		100	$Err_{al} = 9.34\%$	$Err_{al} = 9.25\%$	$Err_{al} = 9.24\%$

Table 6: Layer’s global and local errors for Bonet’s potential for a contrast $c = 2000$

Fig. 12 and table 7 show the same experiments but using the variant of Kaliske’s potential. Overall, it can be seen that the error level is comparable and slightly lower than that for Bonet’s potential, although this does not represent a significant advantage.

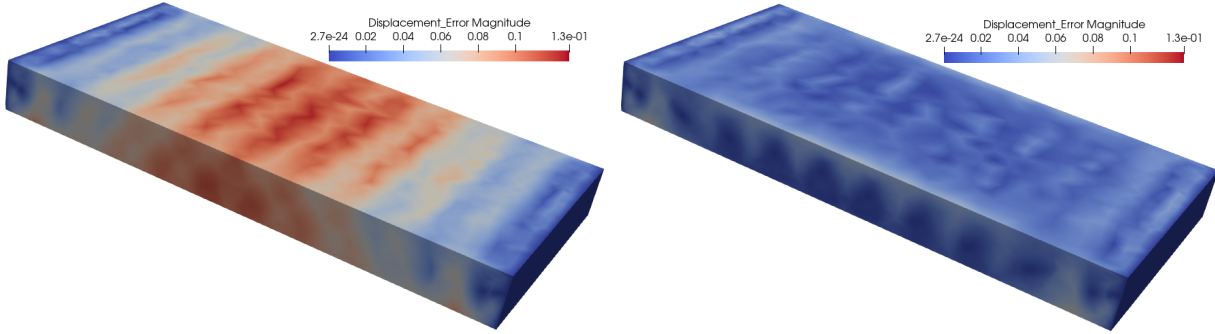


Figure 12: Error distribution before correction for the variant of Kaliske’s potential (left) and after correction (right)

	Before correction	weight	After correction		
			1 iteration	2 iterations	3 iterations
Global error	$Err_g = 8.31\%$	1	$Err_g = 3.24\%$	$Err_g = 3.47\%$	$Err_g = 3.46\%$
		10	$Err_g = 1.65\%$	$Err_g = 1.75\%$	$Err_g = 1.74\%$
		100	$Err_g = 1.72\%$	$Err_g = 1.65\%$	$Err_g = 1.66\%$
Average local error on layer volume elements	$Err_{al} = 18.04\%$	1	$Err_{al} = 12.98\%$	$Err_{al} = 13.14\%$	$Err_{al} = 13.12\%$
		10	$Err_{al} = 9.61\%$	$Err_{al} = 9.82\%$	$Err_{al} = 9.86\%$
		100	$Err_{al} = 9.19\%$	$Err_{al} = 9.32\%$	$Err_{al} = 9.30\%$

Table 7: Layer’s global and local error for Kaliske’s potential variant for a contrast $c = 2000$

These results on the considered experiment, show that quite low levels of error can be reached with both Bonet’s and Kaliske variant potential with the proposed method, at the considered deformation level. Even if Bonet’s potential gives slightly larger errors, it can be a good compromise since the number of parameters to be identified is more restricted than for the Kaliske variant potential (5 instead of 16) which leads to a lower computational cost.

6 Conclusion

The aim of this study was the design of a homogenization procedure having a relatively low computational cost and ensuring a good accuracy in the framework of fiber reinforced layers in large elastic deformations. We presented an iterative method whose numerical cost is intermediate between the decoupled method of Terada et al. [111] and the FE^2 method and tested two isotropic transverse laws, Bonet’s and Kaliske variant’s ones, having a small number of parameter, still in the aim to limit the computational cost.

This method allows a substantial gain in accuracy at a much lower numerical cost than the FE^2 . As a comparison, on the numerical study that we presented on section 5.2, each iteration of our method requires a standard finite element structural computation using the homogenized law, a computation on the RVE for each of the 50 elementary volumes of the layer and the identification of the coefficients of the homogenized law (which is done in an extremely short time). On the contrary, the FE^2 method requires a calculation on the RVE for each Gauss point of the finite element approximation (approximately 20,000 in our case) and for each iteration of the Newton algorithm used to solve the global problem (more or less 10 iterations in our case). This leads us to estimate that our method requires about 1000 times less computing resources than the FE^2 method in this case.

The numerical results in section 5.2 indicate that it is preferable to give large weight to numerical experiments based on the layer deformation. However, the homogenized law obviously cannot be trained solely on these layer deformations, as these can be relatively uniform in terms of deformation and loading and lead to aberrant coefficients. It is therefore necessary to keep a large panel of deformations from the table 1. The choice of the number of deformation patterns and the range of deformation intensities (50 experiments for each of the 6 simple patterns of table 1 and also for 9 additional patterns distributed in a logarithmic scale up to a deformation of 30%) enabled us to obtain a robust identification. Note also that only the experiments in section 3.4 attempt to approximate a case of strict incompressibility for the homogenized law. In this case, the strategy to work with quasi-incompressible laws yielded very satisfactory results. For the test cases in section 4, the materials on the RVE have Poisson’s ratios of 0.49 for the matrix and 0.3 for the fiber. Since the homogenized material has an intermediate Poisson’s ratio, it is quite far from strict incompressibility.

From the presented numerical study, we conclude that original Kaliske’s law is not convenient for high value of contrast of rigidity between the two materials and we propose a variant which allows a better approximation.

Other classes of potentials, even fully parametric ones, could of course be considered in cases the given precision would be insufficient. This would be the case for instance when the complexity of the micro-structure or the level of deformation may induce some instabilities at the microscopic level (for instance with debonding, buckling or micro-fracturing, see [30, 32]).

In this framework, as it is often very difficult to compute reference solutions on a complex heterogeneous structure because of a prohibitive computational cost, the tests on local errors on volume elements of the macroscopic structure allow to have an interesting estimate of the error made by the choice of the homogenized law.

Acknowledgements

The present work is realized as a part of a scientific collaboration with La Manufacture Française des Pneumatiques MICHELIN. The authors are grateful for financial support and rich discussions. It was also financially supported by the Tunis El Manar University and the “PHC Utique” program

of the French Ministry of Foreign Affairs and Ministry of higher education, research and innovation and the Tunisian Ministry of higher education and scientific research in the CMCU project number 22G1123.

References

- [1] ADKINS, J. E., AND RIVLIN, R. S. Large elastic deformations of isotropic materials x. reinforcement by inextensible cords. *Philosophical Transactions of the Royal Society of London. Series A, Mathematical and Physical Sciences* 248, 944 (1955), 201–223.
- [2] BALZANI, D., NEFF, P., SCHRÖDER, J., AND HOLZAPFEL, G. A. A polyconvex framework for soft biological tissues. adjustment to experimental data. *International journal of solids and structures* 43, 20 (2006), 6052–6070.
- [3] BATRA, R. Linear constitutive relations in isotropic finite elasticity. *Journal of Elasticity* 51, 3 (1998), 243–245.
- [4] BATRA, R. Comparison of results from four linear constitutive relations in isotropic finite elasticity. *International Journal of Non-Linear Mechanics* 36, 3 (2001), 421–432.
- [5] BENSOUSSAN, A., LIONS, J.-L., AND PAPANICOLAOU, G. *Asymptotic analysis for periodic structures*, vol. 374. American Mathematical Soc., 2011.
- [6] BOEHLER, J.-P. A simple derivation of representations for non-polynomial constitutive equations in some cases of anisotropy. *ZAMM-Journal of Applied Mathematics and Mechanics/Zeitschrift für Angewandte Mathematik und Mechanik* 59, 4 (1979), 157–167.
- [7] BONET, J., AND BURTON, A. A simple orthotropic, transversely isotropic hyperelastic constitutive equation for large strain computations. *Computer methods in applied mechanics and engineering* 162, 1-4 (1998), 151–164.
- [8] CHAIMOON, K., AND CHINDAPRASIRT, P. An anisotropic hyperelastic model with an application to soft tissues. *European Journal of Mechanics-A/Solids* 78 (2019), 103845.
- [9] CHU, T., AND HASHIN, Z. Plastic behavior of composites and porous media under isotropic stress. *International Journal of Engineering Science* 9, 10 (1971), 971–994.
- [10] CLÉMENT, A., SOIZE, C., AND YVONNET, J. Computational nonlinear stochastic homogenization using a nonconcurrent multiscale approach for hyperelastic heterogeneous microstructures analysis. *International Journal for Numerical Methods in Engineering* 91, 8 (2012), 799–824.
- [11] DE BOTTON, G., AND OREN, T. Analytical and numerical analyses of the micromechanics of soft fibrous connective tissues. *Biomechanics and modeling in mechanobiology* 12, 1 (2013), 151–166.
- [12] DEBOTTON, G., HARITON, I., AND SOCOLSKY, E. Neo-hookean fiber-reinforced composites in finite elasticity. *Journal of the Mechanics and Physics of Solids* 54, 3 (2006), 533–559.
- [13] DEBOTTON, G., HARITON, I., AND SOCOLSKY, E. Neo-hookean fiber-reinforced composites in finite elasticity. *Journal of the Mechanics and Physics of Solids* 54, 3 (2006), 533–559.

- [14] DOGHRI, I., EL GHEZAL, M. I., AND ADAM, L. Finite strain mean-field homogenization of composite materials with hyperelastic-plastic constituents. *International Journal of Plasticity* 81 (2016), 40–62.
- [15] EHLERS, W., AND EIPPER, G. The simple tension problem at large volumetric strains computed from finite hyperelastic material laws. *Acta Mechanica* 130, 1 (1998), 17–27.
- [16] EKRE, F., LARSSON, F., RUNESSON, K., AND JÄNICKE, R. Numerical model reduction with error estimation for computational homogenization of non-linear consolidation. *Computer Methods in Applied Mechanics and Engineering* 389 (2022), 114334.
- [17] ERICKSEN, J., AND RIVLIN, R. Large elastic deformations of homogeneous anisotropic materials. In *Collected Papers of RS Rivlin*. Springer, 1997, pp. 467–487.
- [18] ESHELBY, J. D. The determination of the elastic field of an ellipsoidal inclusion, and related problems. *Proceedings of the royal society of London. Series A. Mathematical and physical sciences* 241, 1226 (1957), 376–396.
- [19] ESHELBY, J. D. The elastic field outside an ellipsoidal inclusion. *Proceedings of the Royal Society of London. Series A. Mathematical and Physical Sciences* 252, 1271 (1959), 561–569.
- [20] FEDERICO, S. Volumetric-distortional decomposition of deformation and elasticity tensor. *Mathematics and mechanics of solids* 15, 6 (2010), 672–690.
- [21] FEYEL, F. Multiscale fe2 elastoviscoplastic analysis of composite structures. *Computational Materials Science* 16, 1-4 (1999), 344–354.
- [22] FEYEL, F., AND CHABOCHE, J.-L. Fe2 multiscale approach for modelling the elastoviscoplastic behaviour of long fibre sic/ti composite materials. *Computer methods in applied mechanics and engineering* 183, 3-4 (2000), 309–330.
- [23] FILLEP, S., MERGHEIM, J., AND STEINMANN, P. Computational homogenization of rope-like technical textiles. *Computational Mechanics* 55, 3 (2015), 577–590.
- [24] FISH, J. Bridging the scales in nano engineering and science. *Journal of Nanoparticle Research* 8, 5 (2006), 577–594.
- [25] FISH, J. *Multiscale methods: bridging the scales in science and engineering*. Oxford University Press on Demand, 2010.
- [26] FLORY, P. Thermodynamic relations for high elastic materials. *Transactions of the Faraday Society* 57 (1961), 829–838.
- [27] FUNG, Y.-C. *Biomechanics: mechanical properties of living tissues*. Springer Science & Business Media, 2013.
- [28] GEERS, M. G., KOUZNETSOVA, V. G., MATOUŠ, K., AND YVONNET, J. Homogenization methods and multiscale modeling: nonlinear problems. *Encyclopedia of Computational Mechanics Second Edition* (2017), 1–34.
- [29] GILCHRIST, M., MURPHY, J. G., PARNELL, W., AND PIERRAT, B. Modelling the slight compressibility of anisotropic soft tissue. *International Journal of Solids and Structures* 51, 23-24 (2014), 3857–3865.

- [30] GRECO, F. A study of stability and bifurcation in micro-cracked periodic elastic composites including self-contact. *International Journal of Solids and Structures* 50, 10 (2013), 1646–1663.
- [31] GRECO, F., LEONETTI, L., PRANNO, A., AND RUDYKH, S. Mechanical behavior of bio-inspired nacre-like composites: A hybrid multiscale modeling approach. *Composite Structures* 233 (2020), 111625.
- [32] GRECO, F., LONETTI, P., LUCIANO, R., BLASI, P. N., AND PRANNO, A. Nonlinear effects in fracture induced failure of compressively loaded fiber reinforced composites. *Composite Structures* 189 (2018), 688–699.
- [33] HASHIN, Z., AND SHTRIKMAN, S. A variational approach to the theory of the elastic behaviour of multiphase materials. *Journal of the Mechanics and Physics of Solids* 11, 2 (1963), 127–140.
- [34] HE, Q.-C. Uniform strain fields and microstructure-independent relations in nonlinear elastic fibrous composites. *Journal of the Mechanics and Physics of Solids* 47, 8 (1999), 1781–1793.
- [35] HE, Q.-C., LE QUANG, H., AND FENG, Z.-Q. Exact results for the homogenization of elastic fiber-reinforced solids at finite strain. *Journal of Elasticity* 83, 2 (2006), 153–177.
- [36] HELFEN, C. E., AND DIEBELS, S. Computational homogenisation of composite plates: consideration of the thickness change with a modified projection strategy. *Computers & Mathematics with Applications* 67, 5 (2014), 1116–1129.
- [37] HELFENSTEIN, J., JABAREEN, M., MAZZA, E., AND GOVINDJEE, S. On non-physical response in models for fiber-reinforced hyperelastic materials. *International Journal of Solids and Structures* 47, 16 (2010), 2056–2061.
- [38] HERNÁNDEZ, J., OLIVER, J., HUESPE, A. E., CAICEDO, M., AND CANTE, J. High-performance model reduction techniques in computational multiscale homogenization. *Computer Methods in Applied Mechanics and Engineering* 276 (2014), 149–189.
- [39] HILL, R. Elastic properties of reinforced solids: some theoretical principles. *Journal of the Mechanics and Physics of Solids* 11, 5 (1963), 357–372.
- [40] HILL, R. On constitutive macro-variables for heterogeneous solids at finite strain. *Proceedings of the Royal Society of London. A. Mathematical and Physical Sciences* 326, 1565 (1972), 131–147.
- [41] HOLZAPFEL, G. A. Nonlinear solid mechanics: a continuum approach for engineering science. *Meccanica* 37, 4 (2002), 489–490.
- [42] HOLZAPFEL, G. A., GASSER, T. C., AND OGDEN, R. W. A new constitutive framework for arterial wall mechanics and a comparative study of material models. *Journal of elasticity and the physical science of solids* 61, 1 (2000), 1–48.
- [43] HOLZAPFEL, G. A., GASSER, T. C., AND OGDEN, R. W. Comparison of a multi-layer structural model for arterial walls with a fung-type model, and issues of material stability. *Journal of biomechanical engineering* 126, 2 (2004), 264–275.

- [44] HORGAN, C. O., AND SACCOMANDI, G. A new constitutive theory for fiber-reinforced incompressible nonlinearly elastic solids. *Journal of the Mechanics and Physics of Solids* 53, 9 (2005), 1985–2015.
- [45] HORGAN, C. O., AND SMAYDA, M. G. The importance of the second strain invariant in the constitutive modeling of elastomers and soft biomaterials. *Mechanics of Materials* 51 (2012), 43–52.
- [46] HOU, Y., MENG, L., LI, G., XIA, L., AND XU, Y. A novel multiscale modeling strategy of the low-velocity impact behavior of plain woven composites. *Composite Structures* 274 (2021), 114363.
- [47] ILTCHEV, A., MARCADON, V., KRUCH, S., AND FOREST, S. Computational homogenisation of periodic cellular materials: application to structural modelling. *International Journal of Mechanical Sciences* 93 (2015), 240–255.
- [48] KALINA, K. A., LINDEN, L., BRUMMUND, J., METSCH, P., AND KÄSTNER, M. Automated constitutive modeling of isotropic hyperelasticity based on artificial neural networks. *Computational Mechanics* 69, 1 (2022), 213–232.
- [49] KALISKE, M. A formulation of elasticity and viscoelasticity for fibre reinforced material at small and finite strains. *Computer methods in applied mechanics and engineering* 185, 2-4 (2000), 225–243.
- [50] LE, B., YVONNET, J., AND HE, Q.-C. Computational homogenization of nonlinear elastic materials using neural networks. *International Journal for Numerical Methods in Engineering* 104, 12 (2015), 1061–1084.
- [51] LI, Q., DILLARD, D. A., AND BATRA, R. C. Kearsley-type instabilities in finite deformations of transversely isotropic and incompressible hyperelastic materials. *International Journal of Solids and Structures* 196 (2020), 171–178.
- [52] LI, X., LIANG, Y., DUAN, Q., SCHREFLER, B., AND DU, Y. A mixed finite element procedure of gradient cosserat continuum for second-order computational homogenisation of granular materials. *Computational Mechanics* 54, 5 (2014), 1331–1356.
- [53] LIGNON, E. *Modélisation multi-échelles de nappes fibrées en compression*. PhD thesis, Ecole Polytechnique X, 2011.
- [54] LOPEZ-PAMIES, O., AND IDIART, M. I. Fiber-reinforced hyperelastic solids: a realizable homogenization constitutive theory. *Journal of Engineering Mathematics* 68, 1 (2010), 57–83.
- [55] MANDEL, J. *Plasticité Classique Et Viscoplasticité: Course Held at the Department of Mechanics of Solids, September-October, 1971*. Springer, 1972.
- [56] MARSDEN, J., AND HUGHES, T. *Mathematical foundations of elasticity*. Dover Publications, 1994.
- [57] MERRILL, A. J. *Deformations of fibre-reinforced materials*. Spencer, 1972.
- [58] MICHEL, J.-C., LOPEZ-PAMIES, O., CASTAÑEDA, P. P., AND TRIANTAFYLIDIS, N. Microscopic and macroscopic instabilities in finitely strained fiber-reinforced elastomers. *Journal of the Mechanics and Physics of Solids* 58, 11 (2010), 1776–1803.

- [59] MIEHE, C., AND BAYREUTHER, C. On multiscale fe analyses of heterogeneous structures: from homogenization to multigrid solvers. *International Journal for Numerical Methods in Engineering* 71, 10 (2007), 1135–1180.
- [60] MONTEIRO, E., HE, Q.-C., AND YVONNET, J. Hyperelastic large deformations of two-phase composites with membrane-type interface. *International journal of engineering science* 49, 9 (2011), 985–1000.
- [61] MONTEIRO, E., YVONNET, J., AND HE, Q.-C. Computational homogenization for nonlinear conduction in heterogeneous materials using model reduction. *Computational Materials Science* 42, 4 (2008), 704–712.
- [62] MOONEY, M. A theory of large elastic deformation. *Journal of applied physics* 11, 9 (1940), 582–592.
- [63] MURPHY, J., AND ROGERSON, G. Modelling slight compressibility for hyperelastic anisotropic materials. *Journal of Elasticity* 131, 2 (2018), 171–181.
- [64] NEMAT-NASSER, S., AND HORI, M. *Micromechanics: overall properties of heterogeneous materials*. Elsevier, 2013.
- [65] NEMAT-NASSER, S., AND HORI, M. *Micromechanics: overall properties of heterogeneous materials*. Elsevier, 2013.
- [66] NEZAMABADI, S., ZAHROUNI, H., AND YVONNET, J. Solving hyperelastic material problems by asymptotic numerical method. *Computational mechanics* 47, 1 (2011), 77–92.
- [67] NGUYEN, V.-D., AND NOELS, L. Computational homogenization of cellular materials. *International Journal of Solids and Structures* 51, 11-12 (2014), 2183–2203.
- [68] NÍ ANNAIDH, A., DESTRADE, M., GILCHRIST, M. D., AND MURPHY, J. G. Deficiencies in numerical models of anisotropic nonlinearly elastic materials. *Biomechanics and modeling in mechanobiology* 12, 4 (2013), 781–791.
- [69] NISHI, S., TERADA, K., AND TEMIZER, I. Isogeometric analysis for numerical plate testing of dry woven fabrics involving frictional contact at meso-scale. *Computational Mechanics* 64, 1 (2019), 211–229.
- [70] NOLAN, D., AND MCGARRY, J. On the compressibility of arterial tissue. *Annals of biomedical engineering* 44, 4 (2016), 993–1007.
- [71] NOLAN, D. R., GOWER, A. L., DESTRADE, M., OGDEN, R. W., AND MCGARRY, J. A robust anisotropic hyperelastic formulation for the modelling of soft tissue. *Journal of the mechanical behavior of biomedical materials* 39 (2014), 48–60.
- [72] OGDEN, R. On the overall moduli of non-linear elastic composite materials. *Journal of the Mechanics and Physics of Solids* 22, 6 (1974), 541–553.
- [73] OGDEN, R. Nearly isochoric elastic deformations: application to rubberlike solids. *Journal of the Mechanics and Physics of Solids* 26, 1 (1978), 37–57.
- [74] OGDEN, R. W. *Non-linear elastic deformations*. Courier Corporation, 1997.

- [75] O'SHEA, D. J., ATTARD, M. M., AND KELLERMANN, D. C. Hyperelastic constitutive modelling for transversely isotropic composites and orthotropic biological tissues. *International Journal of Solids and Structures* 169 (2019), 1–20.
- [76] O'SHEA, D. J., ATTARD, M. M., KELLERMANN, D. C., AND SANSOUR, C. Nonlinear finite element formulation based on invariant-free hyperelasticity for orthotropic materials. *International Journal of Solids and Structures* 185 (2020), 191–201.
- [77] OTERO, F., OLLER, S., AND MARTINEZ, X. Multiscale computational homogenization: review and proposal of a new enhanced-first-order method. *Archives of Computational Methods in Engineering* 25, 2 (2018), 479–505.
- [78] PENCE, T. J. Distortion of anisotropic hyperelastic solids under pure pressure loading: compressibility, incompressibility and near-incompressibility. *Journal of Elasticity* 114, 2 (2014), 251–273.
- [79] PIERRAT, B., MURPHY, J., MACMANUS, D., AND GILCHRIST, M. Finite element implementation of a new model of slight compressibility for transversely isotropic materials. *Computer methods in biomechanics and biomedical engineering* 19, 7 (2016), 745–758.
- [80] PLEWS, J., AND DUARTE, C. Bridging multiple structural scales with a generalized finite element method. *International Journal for Numerical Methods in Engineering* 102, 3-4 (2015), 180–201.
- [81] POREBA-SEBASTJAN, M., AND KUŚ, W. Decoupled homogenization of hyperelastic composite with carbon black inclusion. *Computer Methods in Materials Science* 20, 1 (2020), 14–21.
- [82] QUINTANILLA, R., AND SACCOMANDI, G. The importance of the compatibility of nonlinear constitutive theories with their linear counterparts. *Journal of Applied Mechanics* 74, 3 (2007), 455–460.
- [83] RENARD, J., AND MARMONIER, M. Etude de l'initiation de l'endommagement dans la matrice d'un matériau composite par une méthode d'homogénéisation. *La Recherche aérospatiale*, 6 (1987), 43–51.
- [84] RENARD, Y., AND POULIOS, K. Getfem: Automated FE modeling of multiphysics problems based on a generic weak form language. *ACM Transactions on Mathematical Software (TOMS)* 47, 1 (2020), 1–31.
- [85] RIVLIN, R. Large elastic deformations of isotropic materials. i. fundamental concepts. *Philosophical Transactions of the Royal Society of London. Series A, Mathematical and Physical Sciences* 240, 822 (1948), 459–490.
- [86] RIVLIN, R. Mechanics of large elastic deformations with special reference to rubber. *Nature* 167, 4250 (1951), 590–591.
- [87] RIVLIN, R. S. Large elastic deformations of isotropic materials. ii. some uniqueness theorems for pure, homogeneous deformation. *Philosophical Transactions of the Royal Society of London. Series A, Mathematical and Physical Sciences* 240, 822 (1948), 491–508.

- [88] RIVLIN, R. S. Large elastic deformations of isotropic materials iv. further developments of the general theory. *Philosophical transactions of the royal society of London. Series A, Mathematical and physical sciences* 241, 835 (1948), 379–397.
- [89] RIVLIN, R. S., AND SAUNDERS, D. Large elastic deformations of isotropic materials. vii. experiments on the deformation of rubber. *Philosophical Transactions of the Royal Society of London A: Mathematical, Physical and Engineering Sciences* 243, 865 (1951), 251–288.
- [90] SAITO, R., YAMANAKA, Y., MATSUBARA, S., OKABE, T., MORIGUCHI, S., AND TERADA, K. A decoupling scheme for two-scale finite thermoviscoelasticity with thermal and cure-induced deformations. *International Journal for Numerical Methods in Engineering* 122, 4 (2021), 1133–1166.
- [91] SALVADORI, A., BOSCO, E., AND GRAZIOLI, D. A computational homogenization approach for li-ion battery cells: Part 1—formulation. *Journal of the Mechanics and Physics of Solids* 65 (2014), 114–137.
- [92] SÁNCHEZ-PALENCIA, E. Non-homogeneous media and vibration theory. *Lecture notes in physics* 127 (1980).
- [93] SANCHEZ-PALENCIA, E. Homogenization method for the study of composite media. In *Asymptotic Analysis II*—. Springer, 1983, pp. 192–214.
- [94] SANSOUR, C. On the physical assumptions underlying the volumetric-isochoric split and the case of anisotropy. *European Journal of Mechanics-A/Solids* 27, 1 (2008), 28–39.
- [95] SAUTTER, K. B., MESSMER, M., TESCHEMACHER, T., AND BLETZINGER, K.-U. Limitations of the st. venant-kirchhoff material model in large strain regimes. *International Journal of Non-Linear Mechanics* (2022), 104207.
- [96] SCHRÖDER, J., AND NEFF, P. Invariant formulation of hyperelastic transverse isotropy based on polyconvex free energy functions. *International journal of solids and structures* 40, 2 (2003), 401–445.
- [97] SCHRÖDER, J., AND NEFF, P. Invariant formulation of hyperelastic transverse isotropy based on polyconvex free energy functions. *International journal of solids and structures* 40, 2 (2003), 401–445.
- [98] SCHRÖDER, J., AND NEFF, P. On the construction of polyconvex anisotropic free energy functions. In *IUTAM Symposium on Computational Mechanics of Solid Materials at Large Strains* (2003), Springer, pp. 171–180.
- [99] SCHRÖDER, J., NEFF, P., AND BALZANI, D. A variational approach for materially stable anisotropic hyperelasticity. *International journal of solids and structures* 42, 15 (2005), 4352–4371.
- [100] SEGURADO, J., AND LLORCA, J. Simulation of the deformation of polycrystalline nanostructured ti by computational homogenization. *Computational Materials Science* 76 (2013), 3–11.
- [101] SHU, W., AND STANCIULESCU, I. Multiscale homogenization method for the prediction of elastic properties of fiber-reinforced composites. *International Journal of Solids and Structures* 203 (2020), 249–263.

- [102] SHU, W., AND STANCIULESCU, I. Computational modeling and multiscale homogenization of short fiber composites considering complex microstructure and imperfect interfaces. *Composite Structures* 306 (2023), 116592.
- [103] SIMO, J., TAYLOR, R. L., AND PISTER, K. Variational and projection methods for the volume constraint in finite deformation elasto-plasticity. *Computer methods in applied mechanics and engineering* 51, 1-3 (1985), 177–208.
- [104] SMIT, R. J., BREKELMANS, W. M., AND MEIJER, H. E. Prediction of the mechanical behavior of nonlinear heterogeneous systems by multi-level finite element modeling. *Computer methods in applied mechanics and engineering* 155, 1-2 (1998), 181–192.
- [105] SPENCER, A. J. Continuum theory of the mechanics of fibre-reinforced composites, 1985.
- [106] SU, F., LARSSON, F., AND RUNESSON, K. Computational homogenization of coupled consolidation problems in micro-heterogeneous porous media. *International journal for numerical methods in engineering* 88, 11 (2011), 1198–1218.
- [107] TADMOR, E. B., PHILLIPS, R., AND ORTIZ, M. Mixed atomistic and continuum models of deformation in solids. *Langmuir* 12, 19 (1996), 4529–4534.
- [108] TAKANO, N., ZAKO, M., AND OHNISHI, Y. Macro-micro uncoupled homogenization procedure for microscopic nonlinear behavior analysis of composites. *Journal of the Society of Materials Science, Japan* 45, 6Appendix (1996), 81–86.
- [109] TEMIZER, I., AND WRIGGERS, P. An adaptive method for homogenization in orthotropic nonlinear elasticity. *Computer Methods in Applied Mechanics and Engineering* 196, 35-36 (2007), 3409–3423.
- [110] TERADA, K., HIRAYAMA, N., YAMAMOTO, K., KATO, J., KYOYA, T., MATSUBARA, S., ARAKAWA, Y., UENO, Y., AND MIYANAGA, N. Applicability of micro–macro decoupling scheme to two-scale analysis of fiber-reinforced plastics. *Advanced Composite Materials* 23, 5-6 (2014), 421–450.
- [111] TERADA, K., KATO, J., HIRAYAMA, N., INUGAI, T., AND YAMAMOTO, K. A method of two-scale analysis with micro-macro decoupling scheme: application to hyperelastic composite materials. *Computational Mechanics* 52, 5 (2013), 1199–1219.
- [112] TERADA, K., AND KIKUCHI, N. Nonlinear homogenization method for practical applications. *American Society of Mechanical Engineers, Applied Mechanics Division, AMD* 212 (1995), 1–16.
- [113] TERADA, K., AND KIKUCHI, N. A class of general algorithms for multi-scale analyses of heterogeneous media. *Computer methods in applied mechanics and engineering* 190, 40-41 (2001), 5427–5464.
- [114] TRELOAR, L. The elasticity of a network of long-chain molecules. i. *Transactions of the Faraday Society* 39 (1943), 36–41.
- [115] TRUESDELL, C. The mechanical foundations of elasticity and fluid dynamics. *Journal of Rational Mechanics and Analysis* 1 (1952), 125–300.
- [116] TRUESDELL, C., AND NOLL, W. *The non-linear field theories of mechanics*. Springer, 2004.

- [117] TRUESDELL, C., AND TOUPIN, R. The classical field theories. In *Principles of classical mechanics and field theory/Prinzipien der Klassischen Mechanik und Feldtheorie*. Springer, 1960, pp. 226–858.
- [118] VERGORI, L., DESTRADE, M., MCGARRY, P., AND OGDEN, R. W. On anisotropic elasticity and questions concerning its finite element implementation. *Computational Mechanics* 52, 5 (2013), 1185–1197.
- [119] WANG, M., AND LIU, F. A compressible anisotropic hyperelastic model with I_5 and I_7 strain invariants. *Computer Methods in Biomechanics and Biomedical Engineering* 23, 16 (2020), 1277–1286.
- [120] WEISS, J. A., MAKER, B. N., AND GOVINDJEE, S. Finite element implementation of incompressible, transversely isotropic hyperelasticity. *Computer methods in applied mechanics and engineering* 135, 1-2 (1996), 107–128.
- [121] WIERSZYCKI, M., SZAJEK, K., LODYGOWSKI, T., AND NOWAK, M. A two-scale approach for trabecular bone microstructure modeling based on computational homogenization procedure. *Computational Mechanics* 54, 2 (2014), 287–298.
- [122] WU, W., YANG, Y., ZHENG, H., ZHANG, L., AND ZHANG, N. Numerical manifold computational homogenization for hydro-dynamic analysis of discontinuous heterogeneous porous media. *Computer Methods in Applied Mechanics and Engineering* 388 (2022), 114254.
- [123] YVONNET, J. *Computational homogenization of heterogeneous materials with finite elements*, vol. 258 of *Solid Mechanics and Its Applications*. Springer, London, 2019.
- [124] YVONNET, J., GONZALEZ, D., AND HE, Q.-C. Numerically explicit potentials for the homogenization of nonlinear elastic heterogeneous materials. *Computer Methods in Applied Mechanics and Engineering* 198, 33-36 (2009), 2723–2737.
- [125] YVONNET, J., AND HE, Q.-C. The reduced model multiscale method (r3m) for the nonlinear homogenization of hyperelastic media at finite strains. *Journal of Computational Physics* 223, 1 (2007), 341–368.
- [126] YVONNET, J., MONTEIRO, E., AND HE, Q.-C. Computational homogenization method and reduced database model for hyperelastic heterogeneous structures. *International Journal for Multiscale Computational Engineering* 11, 3 (2013).
- [127] ZHUANG, X., WANG, Q., AND ZHU, H. A 3d computational homogenization model for porous material and parameters identification. *Computational Materials Science* 96 (2015), 536–548.